Wrinkling of soft magneto-active plates

Bin Wu[a,*], Michel Destrade[a]

[a]*School of Mathematics, Statistics and Applied Mathematics, NUI Galway, University Road, Galway, Ireland.*

Abstract

Coupled magneto-mechanical wrinkling has appeared in many scenarios of engineering and biology. Hence, soft magneto-active (SMA) plates buckle when subject to critical uniform magnetic field normal to their wide surface. Here, we provide a systematic analysis of the wrinkling of SMA plates subject to an in-plane mechanical load and a transverse magnetic field. We consider two loading modes: plane-strain loading and uni-axial loading, and two models of magneto-sensitive plates: the neo-Hookean ideal magneto-elastic model and the neo-Hookean magnetization saturation Langevin model. Our analysis relies on the theory of nonlinear magneto-elasticity and the associated linearized theory for superimposed perturbations. We derive the Stroh formulation of the governing equations of wrinkling, and combine it with the surface impedance method to obtain explicitly the bifurcation equations identifying the onset of symmetric and antisymmetric wrinkles. We also obtain analytical expressions of instability in the thin- and thick-plate limits. For thin plates, we make the link with classical Euler buckling solutions. We also perform an exhaustive numerical analysis to elucidate the effects of loading mode, load amplitude, and saturation magnetization on the nonlinear static response and bifurcation diagrams. We find that antisymmetric wrinkling modes always occur before symmetric modes. Increasing the pre-compression or heightening the magnetic field has a destabilizing effect for SMA plates, while the saturation magnetization enhances their stability. We show that the Euler buckling solutions are a good approximation to the exact bifurcation curves for thin plates.

Keywords: Magneto-active plate, finite deformation, saturation magnetization, wrinkling instability, Stroh formulation, Euler buckling

*Corresponding author at: School of Mathematics, Statistics and Applied Mathematics, NUI Galway, University Road, Galway, Ireland.

Email address: bin.wu@nuigalway.ie (Bin Wu)

1. Introduction

Soft magneto-active (SMA) materials, such as magneto-active elastomers, are a particularly promising kind of smart materials that can respond to magnetic field excitation. In general, these SMA materials are prepared by mixing micron-sized magnetizable particles (such as carbonyl iron and neodymium-iron-boron) into a non-magnetic elastomeric matrix such as rubber or silicone (Rigbi and Jilken, 1983; Ginder et al., 2002; Kim et al., 2018). They can then deform significantly under the simple, remote, and reversible actuation of magnetic fields. Moreover, their overall magneto-mechanical properties can be altered actively by applying suitable magnetic fields, thus resulting in tunable vibration and wave characteristics. Owing to these superior magneto-mechanical coupling behaviors, SMA materials have recently attracted considerable academic and industrial interests, prefiguring various potential applications which include remote actuators and sensors (Lanotte et al., 2003; Tian et al., 2011; Kim et al., 2018), soft robotics and biomedical devices (Makarova et al., 2016; Luo et al., 2019; Tang et al., 2019), tunable vibration absorbers (Ginder et al., 2001; Hoang et al., 2010), and tunable wave devices (Yu et al., 2018; Karami Mohammadi et al., 2019).

A challenging problem that arises in the study of SMA materials is how to model the strong nonlinearity and the magneto-mechanical coupling. Thus, a lot of academic interest has been devoted over the years to establish a general theoretical framework of nonlinear magneto-(visco)elasticity in order to describe appropriately the magneto-mechanical response of SMA materials (Tiersten, 1964; Brown, 1966; Pao and Yeh, 1973; Maugin, 1988; Brigadnov and Dorfmann, 2003; Dorfmann and Ogden, 2004; Bustamante, 2010; Destrade and Ogden, 2011; Saxena et al., 2013). Comprehensive reviews regarding the theoretical development of nonlinear magneto-elasticity include those by Kankanala and Triantafyllidis (2004) and Dorfmann and Ogden (2014). Furthermore, homogenization techniques based on micromechanical methods have also been developed to understand the connection between the magneto-active microstructures and the macroscopic physical or mechanical properties of SMA materials (Castañeda and Galipeau, 2011; Galipeau et al., 2014).

In a large variety of practical applications, the mechanical and magnetic loads (prestretch, magnetic field, etc.) influence the working performance of smart systems made of SMA materials and may lead to instability and even failure. In fact, it has long been observed that a magneto-elastic beam or plate in a uniform transverse magnetic field will buckle once

the field reaches a critical value (Moon and Pao, 1968; Miya et al., 1978; Gerbal et al., 2015). On the other hand, local buckling and other instability phenomena can be exploited to realize active pattern switching devices and reconfigurable metamaterials. Hence Psarra et al. (2017, 2019) made use of wrinkling and crinkling instabilities of a thin SMA film bonded on a soft non-magnetic substrate to achieve surface pattern control through a combined action of magnetic field and uni-axial pre-compression. Goshkoderia et al. (2020) investigated experimentally instability-induced pattern evolutions in SMA elastomer composites driven by an applied magnetic field.

Thus, it is vital to theoretically study the stability of SMA structures and composites subject to coupled magneto-mechanical loads, so that we can provide solid guidance for simulations and experiments. From a theoretical point of view, the classical buckling problem of a magneto-elastic beam-plate was first addressed by Moon and Pao (1968), based on the thin-plate theory and the assumption of a linear ferromagnetic material. Pao and Yeh (1973) used a general theory of magneto-elasticity to re-examine this problem and to yield an identical antisymmetric buckling equation for thin plates. Following those works, many investigations looked at the same problem, trying to improve mathematical models to explain the discrepancy between experimental results and theoretical predictions (Wallerstein and Peach, 1972; Popelar, 1972; Dalrymple et al., 1974; Miya et al., 1978; Gerbal et al., 2015; Singh and Onck, 2018). Most of the above-mentioned works employed classical structural models to elucidate the magneto-mechanical coupling problem. More recently, using the theory of nonlinear magneto-elasticity, some researchers have explored the onset of instabilities of different SMA structures, including surface instabilities of isotropic SMA half-spaces (Otténio et al., 2008), buckling modes of rectangular SMA blocks undergoing plane-strain loading (Kankanala and Triantafyllidis, 2008), macroscopic instabilities of anisotropic SMA multilayered structures (Rudykh and Bertoldi, 2013), instabilities of a thin SMA layer resting on a soft non-magnetic substrate (Danas and Triantafyllidis, 2014), and instabilities of a cylindrical membrane (Reddy and Saxena, 2018).

The present work revisits the stability problem of SMA plates subject to an in-plane mechanical load and a uniform transverse magnetic field, and evaluates explicitly the onset of wrinkling instabilities. This work differs from previous works (Pao and Yeh, 1973; Kankanala and Triantafyllidis, 2008) in the following respects. (i) We adopt the nonlinear magneto-elasticity theory and the associated linearized theory developed by Dorfmann and

Ogden (2004) and Otténio et al. (2008) to derive the governing equations of nonlinear static response and the bifurcation equations of wrinkles. These theories introduce a total stress tensor and a modified (or total) energy density function to express constitutive relations in a simple and compact form. (ii) Two mechanical loading modes are considered: plane-strain loading (Fig. 1(b)) and uni-axial loading (Fig. 1(c)). (iii) To overcome the complexity of conventional displacement-based method, we employ the Stroh formulation and the surface impedance method (Su et al., 2018) to obtain explicit expressions of the bifurcation equations of antisymmetric and symmetric wrinkling modes (Fig. 1(d) and 1(e)). (iv) We also manage to derive the explicit bifurcation equations corresponding to the thin- and thick-plate limits, and to establish the thin-plate approximate formulas.

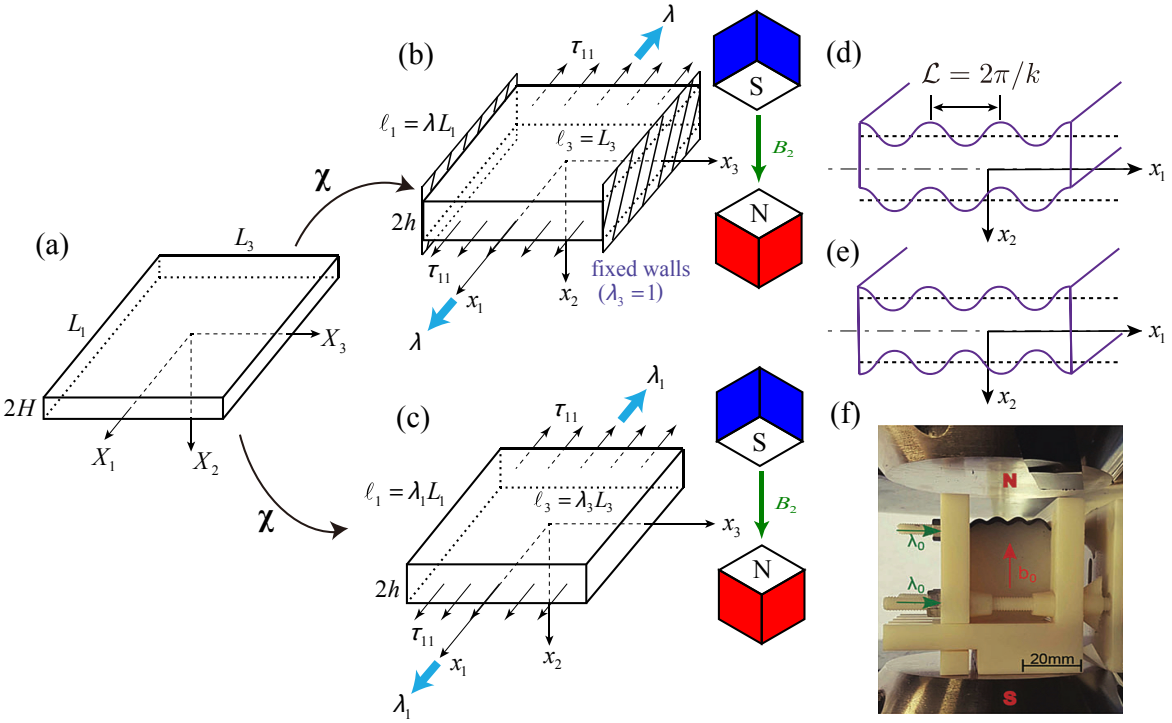

Figure 1: (a)-(e): Schematic diagram of a rectangular SMA plate with Cartesian coordinates and geometry. (a): Undeformed configuration before activation. (b): Deformed configuration subject to plane-strain loading ($\lambda_3 = 1$) with a transverse magnetic field B_2 and (c): Deformed configuration subject to uni-axial loading with a transverse magnetic field B_2 (the magnetic poles are assumed to be very close to the plate, to ensure quasi-uniformity of the mechanical and magnetic fields). (d)-(e): Antisymmetric and symmetric modes of wrinkling instability. (f): Antisymmetric wrinkling due to the application of an external transverse magnetic field to a pre-compressed SMA plate glued onto an inert substrate (taken from Psarra et al. (2017)).

The paper is organized as follows. The equations of nonlinear magneto-elasticity are derived in Sec. 2. The linearized stability analysis is conducted in Sec. 3 to obtain the exact bifurcation equations for symmetric and antisymmetric wrinkles. Section 4 specializes the analytical expressions to the neo-Hookean magnetization saturation material model, including the ideal magneto-elastic model. Numerical calculations are carried out in Sec. 5

to illustrate the effects of loading mode, load amplitude, and saturation magnetization on nonlinear static response and bifurcation diagrams. Section 6 concludes the work with a summary. Some mathematical expressions or derivations are provided in Appendices A-C.

2. Equations of nonlinear magneto-elasticity

2.1. Finite magneto-elasticity theory

We first present the basic equations governing the finite magneto-elastic deformations of an incompressible soft magneto-elastic body, as developed by Dorfmann and Ogden (2004).

In the undeformed stress-free state, the body occupies in the Euclidean space a region $\mathcal{B}_r$ (the boundary being $\partial\mathcal{B}_r$, with the outward normal $\mathbf{N}$), which is taken to be a *reference configuration*. Any material point inside the body is then identified with its position vector $\mathbf{X}$ in $\mathcal{B}_r$. The application of both mechanical load and magnetic field deforms quasistatically the body from $\mathcal{B}_r$ to the *current configuration* $\mathcal{B}$ (the boundary being $\partial\mathcal{B}$, with the outward normal $\mathbf{n}$). The particle located at $\mathbf{X}$ in $\mathcal{B}_r$ now occupies the position $\mathbf{x} = \boldsymbol{\chi}(\mathbf{X})$ in $\mathcal{B}$, where the vector function $\boldsymbol{\chi}$ is a one-to-one, orientation-preserving mapping with a sufficiently regular property. The associated deformation gradient tensor is $\mathbf{F} = \operatorname{Grad}\boldsymbol{\chi} = \partial\boldsymbol{\chi}/\partial\mathbf{X}$ ($F_{i\alpha} = \partial x_i/\partial X_\alpha$ in Cartesian components) with Grad being the gradient operator in $\mathcal{B}_r$. Note that Greek indices are associated with $\mathcal{B}_r$ and Roman indices with $\mathcal{B}$.

The Jacobian of the deformation gradient is $J = \det\mathbf{F}$, and it is equal to 1 at all times for incompressible materials. The left and right Cauchy-Green deformation tensors $\mathbf{b} = \mathbf{F}\mathbf{F}^{\mathrm{T}}$ and $\mathbf{C} = \mathbf{F}^{\mathrm{T}}\mathbf{F}$ are used as the deformation measures, where the superscript $^{\mathrm{T}}$ signifies the transpose.

In the Eulerian description, the equilibrium equations in the absence of mechanical body forces, and the Maxwell equations in the absence of time dependence, free charges and electric currents, are

$$\operatorname{div}\boldsymbol{\tau} = \mathbf{0}, \qquad \operatorname{div}\mathbf{B} = 0, \qquad \operatorname{curl}\mathbf{H} = \mathbf{0}, \tag{1}$$

where $\boldsymbol{\tau}$ is the *total Cauchy stress tensor* including the contribution of magnetic body forces, $\mathbf{B}$ is the Eulerian magnetic induction vector and and $\mathbf{H}$ is the Eulerian magnetic field vector; curl and div are the curl and divergence operators in $\mathcal{B}$, respectively. The conservation of angular momentum implies that $\boldsymbol{\tau}$ is *symmetric*.

The Eulerian magnetization vector $\mathbf{M}$ is defined by the standard relation

$$\mathbf{B} = \mu_0(\mathbf{H} + \mathbf{M}), \tag{2}$$

where $\mu_0 = 4\pi \times 10^{-7}\,\mathrm{N}\cdot\mathrm{A}^{-2}$ is the magnetic permeability in vacuum.

In vacuum, there is no magnetization and Eq. (2) reduces to $\mathbf{B}^\star = \mu_0\mathbf{H}^\star$, where a star superscript identifies a quantity exterior to the material. The *Maxwell stress tensor* $\boldsymbol{\tau}^\star$ in vacuum is

$$\boldsymbol{\tau}^\star = \mu_0^{-1}\left[\mathbf{B}^\star \otimes \mathbf{B}^\star - \tfrac{1}{2}\left(\mathbf{B}^\star \cdot \mathbf{B}^\star\right)\mathbf{I}\right], \tag{3}$$

where $\mathbf{I}$ is the identity tensor. The external fields $\mathbf{B}^\star$ and $\mathbf{H}^\star$ satisfy $\operatorname{div}\mathbf{B}^\star = 0$ and $\operatorname{curl}\mathbf{H}^\star = \mathbf{0}$, which leads to $\operatorname{div}\boldsymbol{\tau}^\star = \mathbf{0}$.

The traction and magnetic boundary conditions are written in Eulerian form as

$$(\boldsymbol{\tau} - \boldsymbol{\tau}^\star)\,\mathbf{n} = \mathbf{t}^{\mathrm{a}}, \qquad (\mathbf{B} - \mathbf{B}^\star)\cdot\mathbf{n} = 0, \qquad (\mathbf{H} - \mathbf{H}^\star)\times\mathbf{n} = \mathbf{0}, \tag{4}$$

where $\mathbf{t}^{\mathrm{a}}$ is the applied mechanical traction vector per unit area of $\partial\mathcal{B}$. Note that the magnetic traction vector $\mathbf{t}^{\mathrm{m}}$ induced by the external Maxwell stress $\boldsymbol{\tau}^\star$ is $\mathbf{t}^{\mathrm{m}} = \boldsymbol{\tau}^\star\mathbf{n}$. Using Nanson's formula, we can transform the governing equations (1) and boundary conditions (4) into the Lagrangian form.

Following the theory of nonlinear magneto-elasticity (Dorfmann and Ogden, 2004), it is convenient to express the nonlinear constitutive relations for incompressible magneto-elastic materials in terms of a *total energy function*, or *modified free energy function*, $\Omega\left(\mathbf{F}, \mathbf{B}_{\mathrm{L}}\right)$ per unit reference volume as

$$\mathbf{T} = \frac{\partial\Omega}{\partial\mathbf{F}} - p\mathbf{F}^{-1}, \qquad \mathbf{H}_{\mathrm{L}} = \frac{\partial\Omega}{\partial\mathbf{B}_{\mathrm{L}}}, \tag{5}$$

where $\mathbf{T} = \mathbf{F}^{-1}\boldsymbol{\tau}$ is the *total* nominal stress tensor, the nominal magnetic field vector $\mathbf{B}_{\mathrm{L}} = \mathbf{F}^{-1}\mathbf{B}$ and the nominal magnetic induction vector $\mathbf{H}_{\mathrm{L}} = \mathbf{F}^{\mathrm{T}}\mathbf{H}$ are the Lagrangian counterparts of $\mathbf{B}$ and $\mathbf{H}$, respectively, and p is a Lagrange multiplier related to the incompressibility constraint, which can be determined from the equilibrium equations and

boundary conditions. The Eulerian counterparts of Eq. (5) are

$$\boldsymbol{\tau} = \mathbf{F}\frac{\partial \Omega}{\partial \mathbf{F}} - p\mathbf{I}, \qquad \mathbf{H} = \mathbf{F}^{-\mathrm{T}}\frac{\partial \Omega}{\partial \mathbf{B}_{\mathrm{L}}}. \tag{6}$$

For an incompressible isotropic material, the energy function Ω can be reduced to a function depending only on the following five invariants:

$$\begin{aligned} &I_1 = \operatorname{tr}\mathbf{C}, && I_2 = \tfrac{1}{2}\left[(\operatorname{tr}\mathbf{C})^2 - \operatorname{tr}\left(\mathbf{C}^2\right)\right], \\ &I_4 = \mathbf{B}_{\mathrm{L}}\cdot\mathbf{B}_{\mathrm{L}}, && I_5 = \mathbf{B}_{\mathrm{L}}\cdot(\mathbf{C}\mathbf{B}_{\mathrm{L}}), && I_6 = \mathbf{B}_{\mathrm{L}}\cdot\left(\mathbf{C}^2\mathbf{B}_{\mathrm{L}}\right). \end{aligned} \tag{7}$$

According to Eqs. (6) and (7), the total Cauchy stress tensor $\boldsymbol{\tau}$ and the Eulerian magnetic field vector $\mathbf{H}$ are then derived as

$$\begin{aligned} \boldsymbol{\tau} &= 2\Omega_1\mathbf{b} + 2\Omega_2\left(I_1\mathbf{b} - \mathbf{b}^2\right) - p\mathbf{I} + 2\Omega_5\mathbf{B}\otimes\mathbf{B} + 2\Omega_6\left(\mathbf{B}\otimes\mathbf{b}\mathbf{B} + \mathbf{b}\mathbf{B}\otimes\mathbf{B}\right), \\ \mathbf{H} &= 2\left(\Omega_4\mathbf{b}^{-1}\mathbf{B} + \Omega_5\mathbf{B} + \Omega_6\mathbf{b}\mathbf{B}\right), \end{aligned} \tag{8}$$

where $\Omega_n = \partial\Omega/\partial I_n$ $(n = 1, 2, 4, 5, 6)$.

2.2. Pure homogeneous deformation of a plate

We now specialize the above equations of nonlinear magneto-elasticity to the homogeneous deformation of an SMA plate subject to an in-plane mechanical load and a uniform magnetic field along its thickness direction. In this work, we consider two mechanical loading modes: plane-strain loading (see Fig. 1(b)) and uni-axial loading (see Fig. 1(c)).

We point out that to simplify the mathematical modelling and obtain explicit analytical solutions to the nonlinear response and the bifurcation criteria of SMA plates, we make the following assumptions. (i) The plate is entirely immersed in the external magnetic field and subjected to an applied uniform magnetic field in the thickness direction. (ii) The plate is of infinite lateral extent, i.e., the plate lateral dimensions are much larger than its thickness. (iii) The magnetic poles are very close to the plate, see Fig. 1(b) and 1(c) for sketches and Fig. 1(f) for the experimental apparatus of Psarra et al. (2017). These assumptions ensure that the field heterogeneity is only confined to the plate edges, while far away from the edges, the induced stress and magnetic field distributions can be envisioned as uniform, which is a good approximation in the sense of Saint-Venant's principle. A similar processing method

has been adopted by Su et al. (2020) to analyze the wrinkling of soft electro-active plates immersed in external electric fields.

Let (X_1, X_2, X_3) and (x_1, x_2, x_3) be the Cartesian coordinates in the reference and current configurations, respectively, along the $(\mathbf{E}_1, \mathbf{E}_2, \mathbf{E}_3)$ and $(\mathbf{e}_1, \mathbf{e}_2, \mathbf{e}_3)$ unit vectors. In the undeformed configuration, the plate has uniform thickness $2H$ along the X_2 direction and lateral lengths L_1, L_3 in the (X_1, X_3) plane. The pure homogeneous deformations corresponding to the two loading modes are defined by $x_1 = \lambda_1 X_1$, $x_2 = \lambda_2 X_2$, $x_3 = \lambda_3 X_3$, where λ_i $(i = 1, 2, 3)$ is the principal stretch in the X_i direction and $\lambda_2 = (\lambda_1\lambda_3)^{-1}$ by incompressibility. The resulting deformation gradient tensor is the diagonal matrix $\mathbf{F} = \text{diag}\left[\lambda_1, (\lambda_1\lambda_3)^{-1}, \lambda_3\right]$ in the $\mathbf{e}_i \otimes \mathbf{E}_j$ basis. The current thickness and lateral lengths of the deformed plate are $2h$, ℓ_1 and ℓ_3, respectively.

We take the underlying Eulerian magnetic induction vector $\mathbf{B}$ to be in the x_2 direction, that is, $\mathbf{B} = [0, B_2, 0]^{\mathrm{T}}$. The associated Lagrangian field $\mathbf{B}_{\mathrm{L}} = \mathbf{F}^{-1}\mathbf{B}$ is $\mathbf{B}_{\mathrm{L}} = [0, B_{\mathrm{L}2}, 0]^{\mathrm{T}}$ with $B_{\mathrm{L}2} = \lambda_1\lambda_3 B_2$. The five independent invariants in Eq. (7) are written now as

$$
\begin{aligned}
&I_1 = \lambda_1^2 + (\lambda_1\lambda_3)^{-2} + \lambda_3^2, \qquad I_2 = \lambda_1^{-2} + \lambda_3^{-2} + \lambda_1^2\lambda_3^2, \\
&I_4 = \lambda_1^2\lambda_3^2 B_2^2, \qquad I_5 = (\lambda_1\lambda_3)^{-2} I_4, \qquad I_6 = (\lambda_1\lambda_3)^{-4} I_4.
\end{aligned} \tag{9}
$$

Thus, we can define a reduced energy function ω as $\omega(\lambda_1, \lambda_3, I_4) = \Omega(I_1, I_2, I_4, I_5, I_6)$. Based on Eq. (9) and the chain rule, the constitutive relations (8) are written as

$$
\tau_{11} - \tau_{22} = \lambda_1\omega_{\lambda_1}, \qquad \tau_{33} - \tau_{22} = \lambda_3\omega_{\lambda_3}, \qquad H_2 = 2(\lambda_1\lambda_3)^2 B_2\omega_4, \tag{10}
$$

where $\omega_{\lambda_1} = \partial\omega/\partial\lambda_1$, $\omega_{\lambda_3} = \partial\omega/\partial\lambda_3$, and $\omega_4 = \partial\omega/\partial I_4$. They satisfy

$$
\begin{aligned}
\lambda_1\omega_{\lambda_1} &= 2\left[\left(\Omega_1 + \Omega_2\lambda_3^2\right)\left(\lambda_1^2 - \lambda_1^{-2}\lambda_3^{-2}\right) - \left(\Omega_5 + 2\Omega_6\lambda_1^{-2}\lambda_3^{-2}\right)B_2^2\right], \\
\lambda_3\omega_{\lambda_3} &= 2\left[\left(\Omega_1 + \Omega_2\lambda_1^2\right)\left(\lambda_3^2 - \lambda_1^{-2}\lambda_3^{-2}\right) - \left(\Omega_5 + 2\Omega_6\lambda_1^{-2}\lambda_3^{-2}\right)B_2^2\right], \\
(\lambda_1\lambda_3)^2\omega_4 &= \Omega_4(\lambda_1\lambda_3)^2 + \Omega_5 + \Omega_6(\lambda_1\lambda_3)^{-2}.
\end{aligned} \tag{11}
$$

Note that $H_1 = H_3 = 0$ from Eq. $(8)_2$. For constant λ_1, λ_3 and B_2, all the fields are uniform and hence satisfy the equilibrium equations and the Maxwell equations automatically.

It follows from the magnetic boundary conditions $(4)_{2,3}$ that the non-zero components of

$\mathbf{B}^\star$ and $\mathbf{H}^\star$ are $B_2^\star = B_2$ and $H_2^\star = \mu_0^{-1} B_2$, respectively. Thus, the non-zero components of the Maxwell stress (3) are

$$\tau_{11}^\star = \tau_{33}^\star = -\tau_{22}^\star = -\tfrac{1}{2}\mu_0^{-1} B_2^2. \tag{12}$$

These Maxwell stress components generate the magnetic traction vector $\mathbf{t}^{\mathrm{m}} = \boldsymbol{\tau}^\star \mathbf{n}$.

For *uni-axial mechanical loading* in the x_1 direction (Fig. 1(c)), there are no mechanical tractions applied on the faces $x_2 = \pm h$ and $x_3 = \pm \ell_3/2$, only magnetic tractions. The traction boundary conditions $(4)_1$ yield

$$\tau_{22} = \tau_{22}^\star, \qquad \tau_{33} = \tau_{33}^\star, \qquad \tau_{11} - \tau_{11}^\star = t_1^{\mathrm{a}} = \lambda_1 s_1, \tag{13}$$

where s_1 is the nominal mechanical traction per unit area of $\partial \mathcal{B}_r$ applied on the faces $x_1 = \pm \ell_1/2$. Thus, we deduce from Eqs. (10) and (13) that the governing equations of the nonlinear response for uni-axial loading are

$$\lambda_1 \omega_{\lambda_1} + \tau_{22}^\star - \tau_{11}^\star = \lambda_1 s_1, \qquad \lambda_3 \omega_{\lambda_3} + \tau_{22}^\star - \tau_{33}^\star = 0, \qquad H_2 = 2(\lambda_1 \lambda_3)^2 B_2 \omega_4, \tag{14}$$

Note that Eq. $(14)_2$ determines the induced principal stretch λ_3 in terms of the stretch λ_1 and magnetic field B_2. Then s_1 and H_2 are calculated from Eqs. $(14)_{1,3}$, respectively.

For *plane-strain mechanical loading* in the x_1 direction (Fig. 1(b)), we have $\lambda_3 = 1$ and $\lambda_1 = \lambda_2^{-1} \equiv \lambda$. There is no mechanical traction applied on the faces $x_2 = \pm h$, but lateral mechanical tractions, applied on the faces $x_1 = \pm \ell_1/2$ and $x_3 = \pm \ell_3/2$, are required to maintain the plane-strain deformation. As a result, Eq. (9) becomes

$$I_1 = I_2 = \lambda^2 + \lambda^{-2} + 1, \qquad I_4 = \lambda^2 B_2^2, \qquad I_5 = \lambda^{-2} I_4, \qquad I_6 = \lambda^{-4} I_4. \tag{15}$$

By introducing the reduced energy function $\tilde{\omega}$ as $\tilde{\omega}(\lambda, I_4) = \Omega(I_1, I_2, I_4, I_5, I_6)$, it follows from the constitutive relations (8) that

$$\begin{aligned} &\tau_{11} - \tau_{22} = \lambda \tilde{\omega}_\lambda, \qquad H_2 = 2\lambda^2 B_2 \tilde{\omega}_4, \\ &\tau_{33} - \tau_{22} = 2\left[\left(\lambda^{-2}\Omega_1 + \Omega_2\right)\left(\lambda^2 - 1\right) - \left(\Omega_5 + 2\lambda^{-2}\Omega_6\right) B_2^2\right], \end{aligned} \tag{16}$$

where $\tilde{\omega}_\lambda = \partial\tilde{\omega}/\partial\lambda$ and $\tilde{\omega}_4 = \partial\tilde{\omega}/\partial I_4$. They are determined by

$$\lambda\tilde{\omega}_\lambda = 2\left[\left(\lambda^2 - \lambda^{-2}\right)(\Omega_1 + \Omega_2) - \left(\Omega_5 + 2\Omega_6\lambda^{-2}\right)B_2^2\right],$$
$$\lambda^2\tilde{\omega}_4 = \lambda^2\Omega_4 + \Omega_5 + \lambda^{-2}\Omega_6. \tag{17}$$

For this loading mode, the traction boundary conditions $(4)_1$ read

$$\tau_{22} = \tau_{22}^\star, \qquad \tau_{11} - \tau_{11}^\star = t_1^{\rm a} = \lambda s_1, \qquad \tau_{33} - \tau_{33}^\star = t_3^{\rm a} = s_3, \tag{18}$$

where s_1 and s_3 are the nominal mechanical tractions applied on the faces $x_1 = \pm\ell_1/2$ and $x_3 = \pm\ell_3/2$, respectively. In view of Eqs. $(16)_{1,2}$ and (18), the nonlinear static response for plane-strain loading is governed by

$$\lambda\tilde{\omega}_\lambda + \tau_{22}^\star - \tau_{11}^\star = \lambda s_1, \qquad \tau_{33} - \tau_{22} + \tau_{22}^\star - \tau_{33}^\star = s_3, \qquad H_2 = 2\lambda^2 B_2\tilde{\omega}_4, \tag{19}$$

where $\tau_{33} - \tau_{22}$ is given by Eq. $(16)_3$. Thus, Eq. (19) is used to calculate s_1, s_3 and H_2 in terms of the applied stretch λ and magnetic field B_2.

3. Linearized stability analysis

In this section we employ the linearized incremental theory of magneto-elasticity (Otténio et al., 2008; Destrade and Ogden, 2011) and the Stroh formalism (Su et al., 2018) to investigate the formation of small-amplitude wrinkles, signaling the onset of wrinkling instability of the SMA plate, for the two loading modes described in Sec. 2.2.

3.1. Incremental governing equations

Consider an infinitesimal incremental mechanical displacement $\mathbf{u} = \dot{\mathbf{x}}$ along with an updated incremental magnetic induction vector $\dot{\mathbf{B}}_{\rm L0}$, superimposed on the finitely deformed configuration reached via $\mathbf{x} = \boldsymbol{\chi}(\mathbf{X})$. Here and henceforth, a superposed dot indicates an increment.

The incremental balance laws and the incremental incompressibility condition are formulated in Eulerian, or updated Lagrangian, form as

$$\operatorname{div}\dot{\mathbf{T}}_0 = \mathbf{0}, \qquad \operatorname{div}\dot{\mathbf{B}}_{\rm L0} = 0, \qquad \operatorname{curl}\dot{\mathbf{H}}_{\rm L0} = \mathbf{0}, \qquad \operatorname{div}\mathbf{u} = \operatorname{tr}\mathbf{L} = 0, \tag{20}$$

where $\dot{\mathbf{T}}_0 = \mathbf{F}\dot{\mathbf{T}}$, $\dot{\mathbf{B}}_{\mathrm{L}0} = \mathbf{F}\dot{\mathbf{B}}_{\mathrm{L}}$ and $\dot{\mathbf{H}}_{\mathrm{L}0} = \mathbf{F}^{-\mathrm{T}}\dot{\mathbf{H}}_{\mathrm{L}}$ are the push-forward versions of the corresponding Lagrangian increments $\dot{\mathbf{T}}$, $\dot{\mathbf{B}}_{\mathrm{L}}$ and $\dot{\mathbf{H}}_{\mathrm{L}}$, respectively, and $\mathbf{L} = \operatorname{grad}\mathbf{u}$ is the incremental displacement gradient. The resulting push-forward quantities are identified with a subscript 0.

The linearized incremental constitutive equations for incompressible SMA materials read

$$\dot{\mathbf{T}}_0 = \boldsymbol{\mathcal{A}}_0\mathbf{L} + \boldsymbol{\Gamma}_0\dot{\mathbf{B}}_{\mathrm{L}0} + p\mathbf{L} - \dot{p}\mathbf{I}, \qquad \dot{\mathbf{H}}_{\mathrm{L}0} = \boldsymbol{\Gamma}_0^{\mathrm{T}}\mathbf{L} + \mathbf{K}_0\dot{\mathbf{B}}_{\mathrm{L}0}, \tag{21}$$

where $\boldsymbol{\mathcal{A}}_0$, $\boldsymbol{\Gamma}_0$ and $\mathbf{K}_0$ are, respectively, fourth-, third- and second-order tensors, which are referred to as *instantaneous* magneto-elastic moduli tensors (see Otténio et al. (2008) and Destrade and Ogden (2011) for their general expressions). In index notation, these magneto-elastic moduli tensors are given by

$$\mathcal{A}_{0piqj} = F_{p\alpha}F_{q\beta}\mathcal{A}_{\alpha i\beta j}, \qquad \Gamma_{0piq} = F_{p\alpha}F^{-1}_{\beta q}\Gamma_{\alpha i\beta}, \qquad K_{0ij} = F^{-1}_{\alpha i}F^{-1}_{\beta j}K_{\alpha\beta}, \tag{22}$$

where $\boldsymbol{\mathcal{A}}$, $\boldsymbol{\Gamma}$ and $\mathbf{K}$ are the relevant *referential* magneto-elastic moduli tensors, which are defined by $\boldsymbol{\mathcal{A}} = \partial^2\Omega/(\partial\mathbf{F}\partial\mathbf{F})$, $\boldsymbol{\Gamma} = \partial^2\Omega/(\partial\mathbf{F}\partial\mathbf{B}_{\mathrm{L}})$, and $\mathbf{K} = \partial^2\Omega/(\partial\mathbf{B}_{\mathrm{L}}\partial\mathbf{B}_{\mathrm{L}})$. Note that the instantaneous moduli tensors have the symmetries $\mathcal{A}_{0piqj} = \mathcal{A}_{0qjpi}$, $\Gamma_{0piq} = \Gamma_{0ipq}$, and $K_{0ij} = K_{0ji}$.

Using the incremental form of the rotational balance condition $\mathbf{FT} = (\mathbf{FT})^{\mathrm{T}}$, we have the following relation between $\boldsymbol{\mathcal{A}}_0$ and $\boldsymbol{\tau}$ for an incompressible material

$$\mathcal{A}_{0jisk} - \mathcal{A}_{0ijsk} = (\tau_{js} + p\delta_{js})\,\delta_{ik} - (\tau_{is} + p\delta_{is})\,\delta_{jk}. \tag{23}$$

The incremental fields exterior to the material read

$$\dot{\mathbf{B}}^\star = \mu_0\dot{\mathbf{H}}^\star, \qquad \dot{\boldsymbol{\tau}}^\star = \mu_0^{-1}[\dot{\mathbf{B}}^\star \otimes \mathbf{B}^\star + \mathbf{B}^\star \otimes \dot{\mathbf{B}}^\star - (\mathbf{B}^\star \cdot \dot{\mathbf{B}}^\star)\mathbf{I}], \tag{24}$$

where $\dot{\mathbf{B}}^\star$ and $\dot{\mathbf{H}}^\star$ are to satisfy $\operatorname{div}\dot{\mathbf{B}}^\star = 0$ and $\operatorname{curl}\dot{\mathbf{H}}^\star = \mathbf{0}$, respectively, and hence $\dot{\boldsymbol{\tau}}^*$ is divergence-free, i.e., $\operatorname{div}\dot{\boldsymbol{\tau}}^\star = \mathbf{0}$.

The mechanical and magnetic boundary conditions for the incremental fields can be

expressed, in updated Lagrangian form, as

$$\begin{aligned}
&\left[\dot{\mathbf{T}}_0^{\mathrm{T}} - \dot{\boldsymbol{\tau}}^{\star} + \boldsymbol{\tau}^{\star}\mathbf{L}^{\mathrm{T}} - (\operatorname{div}\mathbf{u})\,\boldsymbol{\tau}^{\star}\right]\mathbf{n} = \dot{\mathbf{t}}_0^{\mathrm{A}},\\
&\left[\dot{\mathbf{B}}_{\mathrm{L}0} - \dot{\mathbf{B}}^{\star} + \mathbf{L}\mathbf{B}^{\star} - (\operatorname{div}\mathbf{u})\,\mathbf{B}^{\star}\right]\cdot\mathbf{n} = 0,\\
&\left(\dot{\mathbf{H}}_{\mathrm{L}0} - \dot{\mathbf{H}}^{*} - \mathbf{L}^{\mathrm{T}}\mathbf{H}^{*}\right)\times\mathbf{n} = \mathbf{0},
\end{aligned} \tag{25}$$

where $\dot{\mathbf{t}}_0^{\mathrm{A}}\mathrm{d}a = \dot{\mathbf{t}}^{\mathrm{A}}\mathrm{d}A$, with $\mathbf{t}^{\mathrm{A}}$ being the applied mechanical traction vector per unit area of $\partial\mathcal{B}_r$ (i.e., $\mathbf{t}^{\mathrm{A}}\mathrm{d}A = \mathbf{t}^{\mathrm{a}}\mathrm{d}a$). Note that $\mathrm{d}A$ and $\mathrm{d}a$ are area elements of the reference and current configurations, respectively.

In this work we focus on incremental two-dimensional solutions independent of x_3, such that $u_3 = \dot{B}_{\mathrm{L}03} = \dot{H}_{\mathrm{L}03} = 0$, and hence $u_i = u_i(x_1, x_2)$, $\dot{B}_{\mathrm{L}0i} = \dot{B}_{\mathrm{L}0i}(x_1, x_2)$ and $\dot{H}_{\mathrm{L}0i} = \dot{H}_{\mathrm{L}0i}(x_1, x_2)$ for $i = 1, 2$ and $\dot{p} = \dot{p}(x_1, x_2)$.

From Eq. $(20)_3$, the incremental magnetic field vector $\dot{\mathbf{H}}_{\mathrm{L}0}$ is curl-free and thus an incremental magnetic scalar potential $\dot{\varphi}$ can be introduced such that $\dot{\mathbf{H}}_{\mathrm{L}0} = -\mathrm{grad}\dot{\varphi}$, with components

$$\dot{H}_{\mathrm{L}01} = -\dot{\varphi}_{,1}, \qquad \dot{H}_{\mathrm{L}02} = -\dot{\varphi}_{,2}. \tag{26}$$

The incremental balance laws and incompressibility condition $(20)_{1,2,4}$ become

$$\begin{aligned}
&\dot{T}_{011,1} + \dot{T}_{021,2} = 0, \qquad && \dot{T}_{012,1} + \dot{T}_{022,2} = 0,\\
&\dot{B}_{\mathrm{L}01,1} + \dot{B}_{\mathrm{L}02,2} = 0, && u_{1,1} + u_{2,2} = 0.
\end{aligned} \tag{27}$$

For pure homogeneous deformation of the SMA plate subject to the transverse magnetic field, we have $F_{ij} = 0$ for $i \neq j$ and $B_1 = B_3 = 0$. The magneto-elastic moduli tensors $\boldsymbol{\mathcal{A}}_0$, $\boldsymbol{\Gamma}_0$ and $\mathbf{K}_0$ satisfy (Otténio et al., 2008)

$$\begin{aligned}
&\mathcal{A}_{0iijk} = 0, \quad K_{0jk} = 0, \quad \text{for} \quad j \neq k,\\
&\Gamma_{0ii1} = \Gamma_{01ii} = \Gamma_{0ii3} = \Gamma_{03ii} = 0,\\
&\Gamma_{0ijk} = 0, \quad \text{for} \quad i \neq j \neq k \neq i.
\end{aligned} \tag{28}$$

Consequently, using Eqs. (26) and (28), the incremental constitutive relations (21) are written

in terms of $u_i\,(i=1,2)$ and $\dot{\varphi}$ as

$$\begin{aligned}
\dot{T}_{011} &= (c_{11}+p)\,u_{1,1} + c_{12}u_{2,2} + e_{21}\dot{\varphi}_{,2} - \dot{p},\\
\dot{T}_{012} &= (c_{69}+p)\,u_{1,2} + c_{66}u_{2,1} + e_{16}\dot{\varphi}_{,1},\\
\dot{T}_{021} &= (c_{69}+p)\,u_{2,1} + c_{99}u_{1,2} + e_{16}\dot{\varphi}_{,1},\\
\dot{T}_{022} &= (c_{22}+p)\,u_{2,2} + c_{12}u_{1,1} + e_{22}\dot{\varphi}_{,2} - \dot{p},
\end{aligned} \tag{29}$$

and

$$\begin{aligned}
\dot{B}_{\mathrm{L}01} &= e_{16}(u_{2,1}+u_{1,2}) - \mu_{11}\dot{\varphi}_{,1},\\
\dot{B}_{\mathrm{L}02} &= e_{21}u_{1,1} + e_{22}u_{2,2} - \mu_{22}\dot{\varphi}_{,2},
\end{aligned} \tag{30}$$

where the effective material parameters c_{ij}, e_{ij} and μ_{ij} are defined as

$$\begin{aligned}
&\mu_{11} = K_{011}^{-1}, \quad \mu_{22} = K_{022}^{-1}, \quad e_{16} = -\Gamma_{0211}K_{011}^{-1}, \quad e_{21} = -\Gamma_{0112}K_{022}^{-1}, \quad e_{22} = -\Gamma_{0222}K_{022}^{-1},\\
&c_{11} = \mathcal{A}_{01111} + \Gamma_{0112}e_{21}, \quad c_{12} = \mathcal{A}_{01122} + \Gamma_{0112}e_{22}, \quad c_{22} = \mathcal{A}_{02222} + \Gamma_{0222}e_{22},\\
&c_{69} = \mathcal{A}_{01221} + \Gamma_{0211}e_{16}, \quad c_{66} = \mathcal{A}_{01212} + \Gamma_{0211}e_{16}, \quad c_{99} = \mathcal{A}_{02121} + \Gamma_{0211}e_{16}.
\end{aligned} \tag{31}$$

3.2. Stroh formulation and its resolution for plates

The two-dimensional incremental solutions, for the wrinkling instability with sinusoidal shape along the x_1 direction and amplitude variations along the x_2 direction (see Fig. 1(d) and 1(e)), are sought in the form

$$\begin{aligned}
&\left\{u_1, u_2, \dot{\varphi}, \dot{T}_{021}, \dot{T}_{022}, \dot{B}_{\mathrm{L}02}\right\}\\
&\qquad = \Re\left\{\left[k^{-1}\overline{U}_1, k^{-1}\overline{U}_2, \sqrt{G/\mu_0}k^{-1}\overline{\Phi}, \mathrm{i}G\overline{\Sigma}_{21}, \mathrm{i}G\overline{\Sigma}_{22}, \mathrm{i}\sqrt{G\mu_0}\overline{\Delta}\right]\mathrm{e}^{\mathrm{i}kx_1}\right\},
\end{aligned} \tag{32}$$

where $\mathrm{i}=\sqrt{-1}$, $\overline{U}_1$, $\overline{U}_2$, $\overline{\Phi}$, $\overline{\Sigma}_{21}$, $\overline{\Sigma}_{22}$ and $\overline{\Delta}$ are non-dimensional functions of kx_2 only, $k=2\pi/\mathcal{L}$ is the wrinkling wavenumber with $\mathcal{L}$ being the wavelength of the wrinkles, and G is the initial shear modulus (in Pa) of the SMA plate in the absence of magnetic field.

Following a standard derivation procedure (Su et al., 2018, 2019), we can rewrite the incremental governing equations (27), (29) and (30) in the following non-dimensional Stroh

form:

$$\overline{\boldsymbol{\eta}}' = \mathrm{i}\overline{\mathbf{N}}\overline{\boldsymbol{\eta}} = \mathrm{i}\begin{bmatrix} \overline{\mathbf{N}}_1 & \overline{\mathbf{N}}_2 \\ \overline{\mathbf{N}}_3 & \overline{\mathbf{N}}_1^{\dagger} \end{bmatrix} \overline{\boldsymbol{\eta}}, \tag{33}$$

where $\overline{\boldsymbol{\eta}} = \begin{bmatrix} \overline{U}_1 & \overline{U}_2 & \overline{\Phi} & \overline{\Sigma}_{21} & \overline{\Sigma}_{22} & \overline{\Delta} \end{bmatrix}^{\mathrm{T}}$ is the Stroh vector, $\overline{\mathbf{N}}$ is the 6×6 Stroh matrix, the prime denotes differentiation with respect to kx_2, and † signifies the Hermitian operator. In what follows we use the generalized displacement and traction vectors $\overline{\mathbf{U}} = \begin{bmatrix} \overline{U}_1 & \overline{U}_2 & \overline{\Phi} \end{bmatrix}^{\mathrm{T}}$ and $\overline{\mathbf{S}} = \begin{bmatrix} \overline{\Sigma}_{21} & \overline{\Sigma}_{22} & \overline{\Delta} \end{bmatrix}^{\mathrm{T}}$ to express the Stroh vector as $\overline{\boldsymbol{\eta}} = \begin{bmatrix} \overline{\mathbf{U}} & \overline{\mathbf{S}} \end{bmatrix}^{\mathrm{T}}$. For reference, the 3×3 real sub-matrices $\overline{\mathbf{N}}_i\,(i = 1, 2, 3)$ are presented in Appendix A.

For the constant Stroh matrix $\overline{\mathbf{N}}$ considered here, we seek solutions to Eq. (33) in the form,

$$\overline{\boldsymbol{\eta}}\,(kx_2) = \overline{\boldsymbol{\eta}}^0 \mathrm{e}^{\mathrm{i}qkx_2}. \tag{34}$$

Substituting Eq. (34) into Eq. (33) yields an eigenvalue problem $\left(\overline{\mathbf{N}} - q\mathbf{I}\right)\overline{\boldsymbol{\eta}}^0 = \mathbf{0}$, with eigenvalue q and eigenvector $\overline{\boldsymbol{\eta}}^0$. The requirement of non-trivial solutions results in $\det\left(\overline{\mathbf{N}} - q\mathbf{I}\right) = 0$, which gives the following bi-cubic characteristic equation in q:

$$\overline{c}\,\overline{g}\,q^6 + \left[2\overline{b}\overline{g} + \overline{c}\overline{f} + \overline{d}\left(\overline{d} - 2\overline{e}\right)\right]q^4 + \left[\overline{a}\,\overline{g} + 2\overline{b}\,\overline{f} - 2\overline{d}\left(\overline{d} - \overline{e}\right) - \overline{e}^2\overline{f}/\overline{g}\right]q^2 + \overline{a}\overline{f} + \overline{d}^2 = 0, \tag{35}$$

It is clear that the characteristic equation and hence the eigenvalues do not depend on τ_{22} (appearing in the Stroh matrix (A.1)) for any choice of energy density function, despite the presence of external magnetic field.

Thus, the two-dimensional wrinkling solutions to Eq. (33) for an SMA plate are found as

$$\overline{\boldsymbol{\eta}}\,(kx_2) = \begin{bmatrix} \overline{\mathbf{U}}\,(kx_2) \\ \overline{\mathbf{S}}\,(kx_2) \end{bmatrix} = \sum_{j=1}^{6} A_j \overline{\boldsymbol{\eta}}^{(j)} \mathrm{e}^{\mathrm{i}q_j kx_2}. \tag{36}$$

where $A_j\,(j = 1, \ldots, 6)$ are arbitrary constants to be determined, $q_j\,(j = 1, \ldots, 6)$ are the eigenvalues, and $\overline{\boldsymbol{\eta}}^{(j)}\,(j = 1, \ldots, 6)$ are the eigenvectors associated with q_j. The eigenvalues are complex conjugate pairs because of the real coefficients of Eq. (35).

So far, there is no restriction on the specific form of energy density function Ω. To proceed further and demonstrate the possibility of obtaining concise and analytical eigen-equation and eigenvectors, we henceforth consider the magneto-elastic material to be characterized

by the following *Mooney-Rivlin magneto-elastic model*,

$$\Omega = \frac{G\left(1-\beta\right)}{2}\left(I_1 - 3\right) + \frac{G\beta}{2}\left(I_2 - 3\right) + F\left(I_5\right), \tag{37}$$

where F is an arbitrary function of I_5 only and $\beta \in [0,1]$ is a constant. Note that Eq. (37) with $\beta = 0$ reduces to the neo-Hookean magneto-elastic model, including, for example, the ideal model with no saturation and the magnetization saturation Langevin model, which we consider in Sec. 4.

Using Eqs. (37) and (A.5), the dimensionless parameters $\overline{a}-\overline{g}$ in Eq. (A.2) are calculated as

$$\begin{aligned}
&\overline{a} = \lambda_1^2\left(1-\beta\right) + \lambda_1^2\lambda_3^2\beta - 2\overline{B}_2^2\overline{F}_5, \qquad \overline{c} = \lambda_1^{-2}\lambda_3^{-2}\left(1-\beta\right) + \lambda_1^{-2}\beta,\\
&\overline{b} = \frac{1}{2}\left(\lambda_1^{-2}\lambda_3^{-2} + \lambda_1^2\right)\left[\left(1-\beta\right) + \lambda_3^2\beta\right] + \overline{B}_2^2\left(3\overline{F}_5 + 2\overline{B}_2^2\overline{F}_{55}\right),\\
&\overline{d} = -\overline{B}_2, \qquad \overline{e} = -\overline{B}_2\left[1 + \overline{F}_5/\left(\overline{F}_5 + 2\overline{B}_2^2\overline{F}_{55}\right)\right],\\
&\overline{f} = 1/\left(2\overline{F}_5\right), \qquad \overline{g} = 1/\left[2\left(\overline{F}_5 + 2\overline{B}_2^2\overline{F}_{55}\right)\right],
\end{aligned} \tag{38}$$

where $\overline{B}_2 = B_2/\sqrt{G\mu_0}$ is the dimensionless applied magnetic induction; $\overline{F}_5$ and $\overline{F}_{55}$ are defined as

$$\overline{F}_5 = \mu_0 F_5 = \mu_0 \partial F/\partial I_5, \qquad \overline{F}_{55} = G\mu_0^2 F_{55} = G\mu_0^2\partial^2 F/\partial I_5^2. \tag{39}$$

Then we find that the characteristic equation (35) factorizes as

$$\left(q^2+1\right)\left(q^2+\lambda_1^4\lambda_3^2\right)\left(\overline{F}_5 q^2 + \overline{F}_5 + 2\overline{B}_2^2\overline{F}_{55}\right) = 0, \tag{40}$$

which yields six pure imaginary eigenvalues as

$$q_1 = -q_4 = \mathrm{i}p_1, \qquad q_2 = -q_5 = \mathrm{i}p_2, \qquad q_3 = -q_6 = \mathrm{i}p_3, \tag{41}$$

where the real numbers p_1, p_2, and p_3 are

$$p_1 = 1, \qquad p_2 = \lambda_1^2\lambda_3, \qquad p_3 = \sqrt{1 + 2\overline{B}_2^2\overline{F}_{55}/\overline{F}_5}. \tag{42}$$

The associated eigenvectors are derived as

$$\begin{aligned}
\overline{\boldsymbol{\eta}}^{(1)} &= \Big[1,\, \mathrm{i},\, \mathrm{i}\overline{d}/\overline{f},\, \mathrm{i}(2\overline{c}+\overline{d}^2/\overline{f}-\overline{\tau}_{22}),\, \overline{\tau}_{22}-(\overline{a}+\overline{c}+\overline{d}^2/\overline{f}),\, -\overline{d}\Big]^{\mathrm{T}},\\
\overline{\boldsymbol{\eta}}^{(2)} &= \Big[p_2,\, \mathrm{i},\, \mathrm{i}\overline{d}/\overline{f},\, \mathrm{i}(\overline{a}+\overline{c}+2\overline{d}^2/\overline{f}-\overline{\tau}_{22}),\, (\overline{\tau}_{22}-2\overline{c})p_2,\, -\overline{d}p_2\Big]^{\mathrm{T}},\\
\overline{\boldsymbol{\eta}}^{(3)} &= \big[0,\, 0,\, \mathrm{i}p_3,\, \mathrm{i}p_3\overline{d},\, -\overline{d},\, \overline{f}\big]^{\mathrm{T}},\\
\overline{\boldsymbol{\eta}}^{(4)} &= (\overline{\boldsymbol{\eta}}^{(1)})^{*}, \qquad \overline{\boldsymbol{\eta}}^{(5)} = (\overline{\boldsymbol{\eta}}^{(2)})^{*}, \qquad \overline{\boldsymbol{\eta}}^{(6)} = (\overline{\boldsymbol{\eta}}^{(3)})^{*},
\end{aligned} \tag{43}$$

where the asterisk * denotes the complex conjugate. We observe from Eq. (43) that

$$\begin{aligned}
&\overline{\eta}_1^{(j+3)} = \overline{\eta}_1^{(j)}, \qquad \overline{\eta}_2^{(j+3)} = -\overline{\eta}_2^{(j)}, \qquad \overline{\eta}_3^{(j+3)} = -\overline{\eta}_3^{(j)},\\
&\overline{\eta}_4^{(j+3)} = -\overline{\eta}_4^{(j)}, \qquad \overline{\eta}_5^{(j+3)} = \overline{\eta}_5^{(j)}, \qquad \overline{\eta}_6^{(j+3)} = \overline{\eta}_6^{(j)}, \qquad (j=1,2,3)\,,
\end{aligned} \tag{44}$$

where $\overline{\eta}_i^{(j)}$ is the i-th component of the eigenvector $\overline{\boldsymbol{\eta}}^{(j)}$.

3.3. Incremental boundary conditions

We take the applied mechanical traction $\mathbf{t}^{\mathrm{A}}$ as a *dead load* (i.e., $\dot{\mathbf{t}}_0^{\mathrm{A}} = \dot{\mathbf{t}}^{\mathrm{A}} = \mathbf{0}$), so that the general incremental boundary conditions (25) are specialized to the two-dimensional problem at $x_2 = \pm h$, as

$$\begin{aligned}
&\dot{T}_{021} = -\tau_{11}^{\star}u_{2,1} + \dot{\tau}_{21}^{\star}, \qquad &&\dot{T}_{022} = -\tau_{22}^{\star}u_{2,2} + \dot{\tau}_{22}^{\star},\\
&\dot{B}_{\mathrm{L}02} = \dot{B}_2^{\star} - B_2^{\star}u_{2,2}, \qquad &&\dot{H}_{\mathrm{L}01} = \dot{H}_1^{\star} + H_2^{\star}u_{2,1}.
\end{aligned} \tag{45}$$

From $\operatorname{curl}\dot{\mathbf{H}}^{\star} = \mathbf{0}$, we deduce the existence of an incremental magnetic scalar potential $\dot{\varphi}^{\star} = \dot{\varphi}^{\star}(x_1, x_2)$ in vacuum such that

$$\dot{H}_1^{\star} = -\dot{\varphi}_{,1}^{\star}, \qquad \dot{H}_2^{\star} = -\dot{\varphi}_{,2}^{\star}, \qquad \dot{B}_1^{\star} = -\mu_0\dot{\varphi}_{,1}^{\star}, \qquad \dot{B}_2^{\star} = -\mu_0\dot{\varphi}_{,2}^{\star}. \tag{46}$$

Substituting Eq. $(46)_{3,4}$ into $\operatorname{div}\dot{\mathbf{B}}^{\star} = 0$ results in the Laplace equation for $\dot{\varphi}^{\star}$,

$$\dot{\varphi}_{,11}^{\star} + \dot{\varphi}_{,22}^{\star} = 0. \tag{47}$$

To satisfy the decay condition $\dot{\varphi}^{\star} \to 0$ as $x_2 \to \pm\infty$, we take the solutions to Eq. (47) which

are localized near the interfaces $x_2 = \pm h$, as

$$\begin{aligned} \dot{\varphi}^{\star}_{+} &= k^{-1} A^{\star}_{+} \mathrm{e}^{-kx_2} \mathrm{e}^{\mathrm{i}kx_1}, \quad (x_2 > h), \\ \dot{\varphi}^{\star}_{-} &= k^{-1} A^{\star}_{-} \mathrm{e}^{kx_2} \mathrm{e}^{\mathrm{i}kx_1}, \quad (x_2 < -h), \end{aligned} \tag{48}$$

where $A^{\star}_{+}$ and $A^{\star}_{-}$ are arbitrary constants. Thus, the associated incremental Maxwell stress tensor $(24)_2$ has non-zero components

$$\dot{\tau}^{\star}_{11} = \dot{\tau}^{\star}_{33} = -\dot{\tau}^{\star}_{22} = B^{\star}_2 \dot{\varphi}^{\star}_{+,2}, \qquad \dot{\tau}^{\star}_{12} = \dot{\tau}^{\star}_{21} = -B^{\star}_2 \dot{\varphi}^{\star}_{+,1} \tag{49}$$

and

$$\dot{\tau}^{\star}_{11} = \dot{\tau}^{\star}_{33} = -\dot{\tau}^{\star}_{22} = B^{\star}_2 \dot{\varphi}^{\star}_{-,2}, \qquad \dot{\tau}^{\star}_{12} = \dot{\tau}^{\star}_{21} = -B^{\star}_2 \dot{\varphi}^{\star}_{-,1} \tag{50}$$

for $x_2 > h$ and $x_2 < -h$, respectively.

Inserting Eqs. $(26)_1$, (32), $(46)_1$ and $(48)_1$ into the incremental magnetic boundary condition $(45)_4$ at the plate top surface $x_2 = +h$ leads to the relation

$$\overline{A}^{\star}_{+} \mathrm{e}^{-kh} = \overline{\Phi}\,(kh) + \overline{B}_2 \overline{U}_2\,(kh)\,, \tag{51}$$

where $\overline{A}^{\star}_{+} = A^{\star}_{+} \sqrt{\mu_0 / G}$. Using Eqs. (12), (32), $(46)_4$, $(48)_1$, (49) and (51), we write the incremental boundary conditions $(45)_{1-3}$ at $x_2 = +h$ in an impedance form, as

$$\overline{\mathbf{S}}(kh) = \mathrm{i} \overline{\mathbf{Z}}^{\star}_{+} \overline{\mathbf{U}}(kh), \tag{52}$$

where

$$\overline{\mathbf{Z}}^{\star}_{+} = \begin{bmatrix} 0 & \mathrm{i}\overline{B}_2^2/2 & \mathrm{i}\overline{B}_2 \\ -\mathrm{i}\overline{B}_2^2/2 & -\overline{B}_2^2 & -\overline{B}_2 \\ -\mathrm{i}\overline{B}_2 & -\overline{B}_2 & -1 \end{bmatrix} \tag{53}$$

is a surface impedance matrix connecting the vectors $\overline{\mathbf{S}}(kh)$ and $\overline{\mathbf{U}}(kh)$ at the face $x_2 = +h$.

Similarly, at the plate bottom surface $x_2 = -h$, we obtain

$$\overline{A}^{\star}_{-} \mathrm{e}^{-kh} = \overline{\Phi}\,(-kh) + \overline{B}_2 \overline{U}_2\,(-kh)\,, \qquad \overline{A}^{\star}_{-} = A^{\star}_{-} \sqrt{\mu_0 / G}, \tag{54}$$

and

$$\overline{\mathbf{S}}(-kh) = \mathrm{i}\overline{\mathbf{Z}}_{-}^{\star}\,\overline{\mathbf{U}}(-kh), \tag{55}$$

where the surface impedance matrix in the lower half-space is

$$\overline{\mathbf{Z}}_{-}^{\star} = \begin{bmatrix} 0 & \mathrm{i}\overline{B}_2^2/2 & \mathrm{i}\overline{B}_2 \\ -\mathrm{i}\overline{B}_2^2/2 & \overline{B}_2^2 & \overline{B}_2 \\ -\mathrm{i}\overline{B}_2 & \overline{B}_2 & 1 \end{bmatrix}. \tag{56}$$

3.4. Bifurcation equations for wrinkling instabilities

Using Eq. (A.6), we rewrite Eqs. (52) and (55) as

$$\begin{aligned} \begin{bmatrix} \overline{\mathbf{S}}\,(kh) \\ \overline{\mathbf{S}}\,(-kh) \end{bmatrix} &= \mathrm{i}\begin{bmatrix} \overline{\mathbf{Z}}_{+}^{\star} & \mathbf{0} \\ \mathbf{0} & \overline{\mathbf{Z}}_{-}^{\star} \end{bmatrix}\begin{bmatrix} \overline{\mathbf{U}}(kh) \\ \overline{\mathbf{U}}(-kh) \end{bmatrix} \\ &= \mathrm{i}\begin{bmatrix} \overline{\mathbf{Z}}_{+}^{\star} & \mathbf{0} \\ \mathbf{0} & \overline{\mathbf{Z}}_{-}^{\star} \end{bmatrix}\begin{bmatrix} \overline{\eta}_1^{(1)}E_1^{+} & \overline{\eta}_1^{(2)}E_2^{+} & \overline{\eta}_1^{(3)}E_3^{+} & \overline{\eta}_1^{(4)}E_1^{-} & \overline{\eta}_1^{(5)}E_2^{-} & \overline{\eta}_1^{(6)}E_3^{-} \\ \overline{\eta}_2^{(1)}E_1^{+} & \overline{\eta}_2^{(2)}E_2^{+} & \overline{\eta}_2^{(3)}E_3^{+} & \overline{\eta}_2^{(4)}E_1^{-} & \overline{\eta}_2^{(5)}E_2^{-} & \overline{\eta}_2^{(6)}E_3^{-} \\ \overline{\eta}_3^{(1)}E_1^{+} & \overline{\eta}_3^{(2)}E_2^{+} & \overline{\eta}_3^{(3)}E_3^{+} & \overline{\eta}_3^{(4)}E_1^{-} & \overline{\eta}_3^{(5)}E_2^{-} & \overline{\eta}_3^{(6)}E_3^{-} \\ \overline{\eta}_1^{(1)}E_1^{-} & \overline{\eta}_1^{(2)}E_2^{-} & \overline{\eta}_1^{(3)}E_3^{-} & \overline{\eta}_1^{(4)}E_1^{+} & \overline{\eta}_1^{(5)}E_2^{+} & \overline{\eta}_1^{(6)}E_3^{+} \\ \overline{\eta}_2^{(1)}E_1^{-} & \overline{\eta}_2^{(2)}E_2^{-} & \overline{\eta}_2^{(3)}E_3^{-} & \overline{\eta}_2^{(4)}E_1^{+} & \overline{\eta}_2^{(5)}E_2^{+} & \overline{\eta}_2^{(6)}E_3^{+} \\ \overline{\eta}_3^{(1)}E_1^{-} & \overline{\eta}_3^{(2)}E_2^{-} & \overline{\eta}_3^{(3)}E_3^{-} & \overline{\eta}_3^{(4)}E_1^{+} & \overline{\eta}_3^{(5)}E_2^{+} & \overline{\eta}_3^{(6)}E_3^{+} \end{bmatrix}\begin{bmatrix} A_1 \\ A_2 \\ A_3 \\ A_4 \\ A_5 \\ A_6 \end{bmatrix}. \end{aligned} \tag{57}$$

Substituting Eqs. (44) and (A.7) into Eq. (57) yields

$$\begin{bmatrix} D_1E_1^{+} & D_2E_2^{+} & D_3E_3^{+} & -D_1E_1^{-} & -D_2E_2^{-} & -D_3E_3^{-} \\ F_1^{+}E_1^{+} & F_2^{+}E_2^{+} & F_3^{+}E_3^{+} & F_1^{-}E_1^{-} & F_2^{-}E_2^{-} & F_3^{-}E_3^{-} \\ G_1^{+}E_1^{+} & G_2^{+}E_2^{+} & G_3^{+}E_3^{+} & G_1^{-}E_1^{-} & G_2^{-}E_2^{-} & G_3^{-}E_3^{-} \\ D_1E_1^{-} & D_2E_2^{-} & D_3E_3^{-} & -D_1E_1^{+} & -D_2E_2^{+} & -D_3E_3^{+} \\ F_1^{-}E_1^{-} & F_2^{-}E_2^{-} & F_3^{-}E_3^{-} & F_1^{+}E_1^{+} & F_2^{+}E_2^{+} & F_3^{+}E_3^{+} \\ G_1^{-}E_1^{-} & G_2^{-}E_2^{-} & G_3^{-}E_3^{-} & G_1^{+}E_1^{+} & G_2^{+}E_2^{+} & G_3^{+}E_3^{+} \end{bmatrix}\begin{bmatrix} A_1 \\ A_2 \\ A_3 \\ A_4 \\ A_5 \\ A_6 \end{bmatrix} = 0, \tag{58}$$

where

$$
\begin{aligned}
D_j &= \overline{\eta}_4^{(j)} + \overline{B}_2\left(\overline{B}_2\overline{\eta}_2^{(j)} + 2\overline{\eta}_3^{(j)}\right)/2,\\
F_j^{\pm} &= \overline{\eta}_5^{(j)} - \overline{B}_2^2\overline{\eta}_1^{(j)}/2 \pm \mathrm{i}\overline{B}_2\left(\overline{B}_2\overline{\eta}_2^{(j)} + \overline{\eta}_3^{(j)}\right),\\
G_j^{\pm} &= \overline{\eta}_6^{(j)} - \overline{B}_2\overline{\eta}_1^{(j)} \pm \mathrm{i}\left(\overline{B}_2\overline{\eta}_2^{(j)} + \overline{\eta}_3^{(j)}\right), \quad (j=1,2,3).
\end{aligned}
\tag{59}
$$

By conducting some simple linear matrix manipulations of Eq. (58) and using the relations $E_j^+ + E_j^- = 2\cosh(p_j kh)$ and $E_j^+ - E_j^- = -2\sinh(p_j kh)$, we obtain two sets of independent linear algebraic equations,

$$
\mathbf{P}^{\mathrm{sym}}\begin{bmatrix} A_1 + A_4 \\ A_2 + A_5 \\ A_3 + A_6 \end{bmatrix} = 0, \qquad \mathbf{P}^{\mathrm{anti}}\begin{bmatrix} A_1 - A_4 \\ A_2 - A_5 \\ A_3 - A_6 \end{bmatrix} = 0,
\tag{60}
$$

where the 3×3 coefficient matrices $\mathbf{P}^{\mathrm{sym}}$ and $\mathbf{P}^{\mathrm{anti}}$ have non-zero components

$$
\begin{aligned}
P_{1j}^{\mathrm{sym}} &= \left[\overline{\eta}_4^{(j)} + \overline{B}_2\left(\overline{B}_2\overline{\eta}_2^{(j)} + 2\overline{\eta}_3^{(j)}\right)/2\right]\tanh(p_j kh),\\
P_{2j}^{\mathrm{sym}} &= \left(\overline{\eta}_5^{(j)} - \overline{B}_2^2\overline{\eta}_1^{(j)}/2\right) - \mathrm{i}\overline{B}_2\left(\overline{B}_2\overline{\eta}_2^{(j)} + \overline{\eta}_3^{(j)}\right)\tanh(p_j kh),\\
P_{3j}^{\mathrm{sym}} &= \left(\overline{\eta}_6^{(j)} - \overline{B}_2\overline{\eta}_1^{(j)}\right) - \mathrm{i}\left(\overline{B}_2\overline{\eta}_2^{(j)} + \overline{\eta}_3^{(j)}\right)\tanh(p_j kh),
\end{aligned}
\tag{61}
$$

and

$$
\begin{aligned}
P_{1j}^{\mathrm{anti}} &= \overline{\eta}_4^{(j)} + \overline{B}_2\left(\overline{B}_2\overline{\eta}_2^{(j)} + 2\overline{\eta}_3^{(j)}\right)/2,\\
P_{2j}^{\mathrm{anti}} &= \left(\overline{\eta}_5^{(j)} - \overline{B}_2^2\overline{\eta}_1^{(j)}/2\right)\tanh(p_j kh) - \mathrm{i}\overline{B}_2\left(\overline{B}_2\overline{\eta}_2^{(j)} + \overline{\eta}_3^{(j)}\right),\\
P_{3j}^{\mathrm{anti}} &= \left(\overline{\eta}_6^{(j)} - \overline{B}_2\overline{\eta}_1^{(j)}\right)\tanh(p_j kh) - \mathrm{i}\left(\overline{B}_2\overline{\eta}_2^{(j)} + \overline{\eta}_3^{(j)}\right),
\end{aligned}
\tag{62}
$$

for $j = 1, 2, 3$. For non-trivial solutions of Eq. (60), the determinants of coefficient matrices must vanish, i.e.,

$$
\det\left(\mathbf{P}^{\mathrm{sym}}\right) = 0, \qquad \det\left(\mathbf{P}^{\mathrm{anti}}\right) = 0,
\tag{63}
$$

which identify, respectively, possible symmetric and antisymmetric wrinkling modes.

Substituting Eqs. (A.4), (38), $(42)_{1,2}$ and $(43)_{1,2,3}$ into Eqs. (61)-(63) and with the help

of Mathematica (Wolfram Research, Inc., 2013), we are able to obtain the *explicit bifurcation equation for antisymmetric modes* as

$$\left[1+\beta\left(\lambda_3^2-1\right)\right]\left[2\overline{F}_5 p_3+\tanh\left(p_3 kh\right)\right]\times \\ \left[\left(1+\lambda_1^4\lambda_3^2\right)^2\tanh\left(kh\right)-4\lambda_1^2\lambda_3\tanh\left(\lambda_1^2\lambda_3 kh\right)\right] \\ =\lambda_1^2\lambda_3^2\left(\lambda_1^4\lambda_3^2-1\right)\overline{B}_2^2\left(1-2\overline{F}_5\right)^2\tanh\left(p_3 kh\right), \quad (64)$$

where $kh=\lambda_1^{-1}\lambda_3^{-1}kH$. The bifurcation equation for symmetric modes is the same as Eq. (64) except that tanh is replaced by coth everywhere. Note that Eq. (64) is applicable to both the uni-axial and plane-strain loading considered in Sec. 2.2.

In the *thick-plate* or *short-wave* limit ($kH\to\infty$), the tanh functions in Eq. (64) are replaced by 1 and the bifurcation criteria for both symmetric and antisymmetric modes reduce to

$$\left[1+\beta\left(\lambda_3^2-1\right)\right]\left(1+2\overline{F}_5 p_3\right)\left[\left(\lambda_1^2\lambda_3\right)^3+\left(\lambda_1^2\lambda_3\right)^2+3\lambda_1^2\lambda_3-1\right] \\ =\lambda_1^2\lambda_3^2\left(\lambda_1^2\lambda_3+1\right)\overline{B}_2^2\left(1-2\overline{F}_5\right)^2. \quad (65)$$

Note that the bifurcation equation (65) identifies the surface wrinkling instability for the magneto-elastic half-space, which can also be derived based on the surface impedance method shown in Appendix B. For $\overline{B}_2=0$, Eq. (65) reduces to $\left(\lambda_1^2\lambda_3\right)^3+\left(\lambda_1^2\lambda_3\right)^2+3\lambda_1^2\lambda_3-1=0$, corresponding to the surface instability of a purely elastic half-space (Flavin, 1963).

In the *thin-plate* or *long-wave* limit ($kH\to 0$), we find that the antisymmetric bifurcation equation (64) can be rearranged as

$$2\overline{F}_5\left(\lambda_1^2-\lambda_1^{-2}\lambda_3^{-2}\right)\left[1+\beta\left(\lambda_3^2-1\right)\right]=\overline{B}_2^2\left(1-2\overline{F}_5\right)^2. \quad (66)$$

For $\overline{B}_2=0$, Eq. (66) recovers the critical buckling condition $\lambda_1^2\lambda_3=1$ for the purely elastic case, which results in $\lambda_1^{\rm cr}=1.0$ for both the uni-axial and plane-strain loading. This indicates that in the absence of magnetic field, the infinite-long plate or thin-plate buckles immediately when subject to an extremely small in-plane compression.

4. Specialization to the neo-Hookean magneto-elastic solid

For definiteness, we now specialize the previous results to the neo-Hookean ($\beta = 0$) ideal magneto-elastic model and the neo-Hookean magnetization saturation Langevin model, which are characterized by the following energy functions, respectively,

$$\Omega = \frac{G}{2}\left(I_1 - 3\right) + \frac{1-\chi}{2\mu_0} I_5, \tag{67}$$

and

$$\Omega = \frac{G}{2}\left(I_1 - 3\right) + \frac{I_5}{2\mu_0} + \frac{\mu_0 (m^s)^2}{3\chi}\left\{\ln\left(\frac{3\chi\sqrt{I_5}}{\mu_0 m^s}\right) - \ln\left[\sinh\left(\frac{3\chi\sqrt{I_5}}{\mu_0 m^s}\right)\right]\right\}, \tag{68}$$

where m^s is the saturation magnetization and χ is the magnetic susceptibility that is associated with the relative magnetic permeability μ_r by $\mu_r = 1/(1-\chi)$.

The neo-Hookean ideal model (67) has been used to study the stability of anisotropic magnetorheological elastomers in finite deformations (Rudykh and Bertoldi, 2013). The compressible counterpart of the neo-Hookean magnetization saturation Langevin model (68) has been adopted to investigate instability-induced pattern evolutions of the heterogeneous materials and structures (Psarra et al., 2017, 2019; Goshkoderia et al., 2020).

Note that the magneto-elastic material models (67) and (68) take no account of particle-particle interactions and thus neglect magneto-mechanical coupling in terms of pure material magnetostriction. However, it is emphasized that the neo-Hookean magnetization saturation model (68) allows for a satisfactory quantitative and very good qualitative agreement with the experimental data presented in previous works (Psarra et al., 2017, 2019; Goshkoderia et al., 2020), although it is anticipated to be less accurate in the post-bifurcation regime, especially when wrinkles develop substantially due to the large shear strains. As a result, more elaborate magneto-mechanical models such as the ones proposed recently by Mukherjee et al. (2020) are required to explore the effects of the strain-stiffening and the constituent phase properties (such as particle volume fraction, particle-particle interactions, etc) on the wrinkling instability of SMA structures, but such models are out of the scope of this paper.

Using Eqs. (2), $(8)_2$ and (67) or (68), we get the governing equations of the magnetization response

$$\mathbf{M} = \mu_0^{-1}\chi\mathbf{B} \tag{69}$$

for the ideal model, and

$$\mathbf{M}=\left[\frac{m^s}{|\mathbf{B}|}\coth\left(\frac{3\chi\,|\mathbf{B}|}{\mu_0 m^s}\right)-\frac{\mu_0(m^s)^2}{3\chi|\mathbf{B}|^2}\right]\mathbf{B} \tag{70}$$

for the saturation Langevin model. In the limit of small magnetic field ($\mathbf{B}\to\mathbf{0}$), one can verify that the saturation magnetization response (70) is compatible with the linear magnetization response (69).

Now introduce the following dimensionless quantities in terms of the initial shear modulus G and the vacuum magnetic permeability μ_0:

$$\begin{aligned}&\overline{I}_5=\frac{I_5}{G\mu_0}=\overline{B}_2^2,\qquad \overline{M}_2=M_2\sqrt{\frac{\mu_0}{G}},\qquad \overline{m}^s=m^s\sqrt{\frac{\mu_0}{G}},\\&\overline{s}_1=\frac{s_1}{G},\qquad \overline{s}_3=\frac{s_3}{G},\qquad \overline{\tau}_{11}=\frac{\tau_{11}}{G},\qquad \overline{\tau}_{33}=\frac{\tau_{33}}{G}.\end{aligned} \tag{71}$$

Inserting Eqs. (67) and (68) into Eq. (39) gives

$$\overline{F}_5=(1-\chi)/2,\qquad \overline{F}_{55}=0 \tag{72}$$

for the ideal model, and

$$\begin{aligned}\overline{F}_5&=\frac{1}{2}\left[1+\frac{(\overline{m}^s)^2}{3\chi\overline{I}_5}-\frac{\overline{m}^s}{\sqrt{\overline{I}_5}}\coth\left(\frac{3\chi}{\overline{m}^s}\sqrt{\overline{I}_5}\right)\right],\\\overline{F}_{55}&=\frac{1}{2}\left[-\frac{(\overline{m}^s)^2}{3\chi\overline{I}_5^2}+\frac{\overline{m}^s}{2\overline{I}_5^{3/2}}\coth\left(\frac{3\chi\sqrt{\overline{I}_5}}{\overline{m}^s}\right)+\frac{3\chi}{2\overline{I}_5}\sinh^{-2}\left(\frac{3\chi\sqrt{\overline{I}_5}}{\overline{m}^s}\right)\right]\end{aligned} \tag{73}$$

for the saturation Langevin model.

Thus, the magnetization responses (69) and (70) to the applied transverse magnetic field are written in non-dimensional form, as

$$M_2^\star=\left(1-2\overline{F}_5\right)B_2^\star, \tag{74}$$

where $B_2^\star\equiv B_2/(\mu_0 m^s)=\overline{B}_2/\overline{m}^s$ and $M_2^\star\equiv M_2/m^s=\overline{M}_2/\overline{m}^s$.

Substituting Eqs. (67) and (68) into Eqs. $(11)_{1,2}$, $(16)_3$ and $(17)_1$, we obtain the nonlinear mechanical response from Eqs. $(14)_{1,2}$ and $(19)_{1,2}$ as

$$\lambda_1^2-\lambda_1^{-2}\lambda_3^{-2}+\left(1-2\overline{F}_5\right)\overline{B}_2^2=\lambda_1\overline{s}_1,\qquad \lambda_3^2-\lambda_1^{-2}\lambda_3^{-2}+\left(1-2\overline{F}_5\right)\overline{B}_2^2=0 \tag{75}$$

for uni-axial loading, and

$$\lambda^2 - \lambda^{-2} + \left(1 - 2\overline{F}_5\right)\overline{B}_2^2 = \lambda\overline{s}_1, \qquad \overline{s}_3 = 1 - \lambda^{-2} + \left(1 - 2\overline{F}_5\right)\overline{B}_2^2 \tag{76}$$

for plane-strain loading. Practically, we determine the response by prescribing the pre-stretch λ_1 or λ and solving (75) for $\overline{s}_1$ and λ_3 (uni-axial loading) or solving (76) for $\overline{s}_1$ and $\overline{s}_3$ (plane-strain loading).

For the neo-Hookean saturation Langevin model, the bifurcation or buckling equations (64)-(66) are the same except that $\beta = 0$ and $\overline{F}_5$ and $\overline{F}_{55}$ are given in Eq. (73).

For the neo-Hookean ideal model, we find from Eqs. $(42)_3$ and (72) that $p_3 = 1$. As a result, the bifurcation equation (64) reduces to

$$\begin{aligned}\left[1 - \chi + \tanh\left(kh\right)\right]\left[\left(1 + \lambda_1^4\lambda_3^2\right)^2 \tanh\left(kh\right) - 4\lambda_1^2\lambda_3 \tanh\left(\lambda_1^2\lambda_3 kh\right)\right] \\ = \overline{B}_2^2\chi^2\lambda_1^2\lambda_3^2\left(\lambda_1^4\lambda_3^2 - 1\right)\tanh\left(kh\right).\end{aligned} \tag{77}$$

Equations (65) and (66) become

$$\left(2 - \chi\right)\left[\left(\lambda_1^2\lambda_3\right)^3 + \left(\lambda_1^2\lambda_3\right)^2 + 3\lambda_1^2\lambda_3 - 1\right] = \overline{B}_2^2\chi^2\lambda_1^2\lambda_3^2\left(\lambda_1^2\lambda_3 + 1\right) \tag{78}$$

for the thick-plate limit ($kH \to \infty$), and

$$\left(1 - \chi\right)\left(\lambda_1^2 - \lambda_1^{-2}\lambda_3^{-2}\right) = \overline{B}_2^2\chi^2 \tag{79}$$

for the thin-plate limit ($kH \to 0$).

5. Results and discussion

We first conduct numerical calculations in Sec. 5.1 to investigate quantitatively the non-linear static response of incompressible SMA plates subject to mechanical and magnetic loads. Section 5.2 then focuses on the bifurcation analysis to calculate the critical mechanical and/or magnetic field generating the wrinkling instability.

We consider two different loading modes (plane-strain and uni-axial loading) and two neo-Hookean magneto-elastic models ((67) and (68)). The material properties used in the numerical computations are taken as $G = 10$ kPa, $\chi = 0.4$ and $\mu_0 m^s = 0.5$ T, which are

obtained from experiments with a class of magnetorheological elastomers (Psarra et al., 2017, 2019) consisting of a soft silicone mixed with iron particles at a volume fraction of 20%. More details about the fabrication technique can be found in the paper by Psarra et al. (2017).

5.1. Nonlinear static response

The nonlinear static response of an SMA plate subject to mechanical and magnetic loads is calculated from Eqs. (74)-(76).

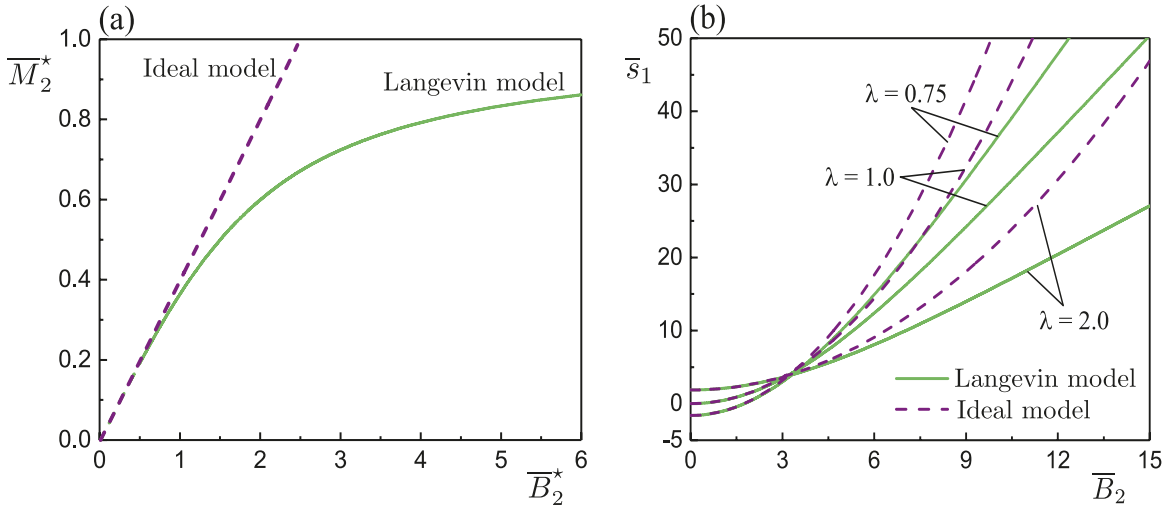

Figure 2: Plane-strain loading: (a) magnetization response of the dimensionless magnetization $M_2^\star = \overline{M}_2/\overline{m}^s$ versus the dimensionless magnetic induction field $B_2^\star = \overline{B}_2/\overline{m}^s$ from Eq. (74); (b) response of the dimensionless nominal mechanical traction $\overline{s}_1$ versus the dimensionless magnetic induction field $\overline{B}_2$ from Eq. $(76)_1$ for three different values of pre-stretch $\lambda = 0.75, 1.0, 2.0$. Solid lines correspond to the ideal magneto-elastic model while dashed lines represent the saturation Langevin model.

For plane-strain loading, Fig. 2(a) shows the magnetization response of the dimensionless magnetization $M_2^\star = \overline{M}_2/\overline{m}^s$ versus the dimensionless magnetic induction field $B_2^\star = \overline{B}_2/\overline{m}^s$ (see Eq. (74)) for the two material models (67) and (68). We see from Fig. 2(a) that a neo-Hookean ideal magneto-elastic plate exhibits a linear magnetization response, whereas the response of a plate with magnetization saturation is nonlinear. The magnetization responses of the two material models are essentially identical for $\overline{B}_2^\star \leq 1.0$ (i.e., $\overline{B}_2 \leq 4.46$). The magnetization begins to saturate at $\overline{B}_2^\star \simeq 6.0$ (i.e., $\overline{B}_2 \simeq 26.76$). We note from Eqs. $(73)_1$ and (74) that the magnetization response of each material model is independent of the mechanical stretch ratio.

For plane-strain loading, the effect of the magnetic induction field $\overline{B}_2$ on the nominal mechanical traction $\overline{s}_1$ applied to the SMA plate is plotted in Fig. 2(b) for three different values of pre-stretch $\lambda = 0.75, 1.0, 2.0$. Clearly, when $\overline{B}_2$ increases, the required mechanical traction increases monotonically, which indicates that the SMA plate has an in-plane con-

traction trend because of the increasing external Maxwell stress. For the three pre-stretches $\lambda = 0.75, 1.0, 2.0$, the mechanical tractions corresponding to the two material models overlap up to $\overline{B}_2 \simeq 3.8, 4.2, 5.0$, respectively. However, the difference predicted by the two material models becomes more evident with subsequent increases in $\overline{B}_2$. Specifically, at the same level of $\overline{B}_2$, the plate with saturation magnetization effect requires a smaller mechanical traction as compared to the ideal magneto-elastic plate. This is because the presence of saturation magnetization will induce a smaller in-plane contraction trend.

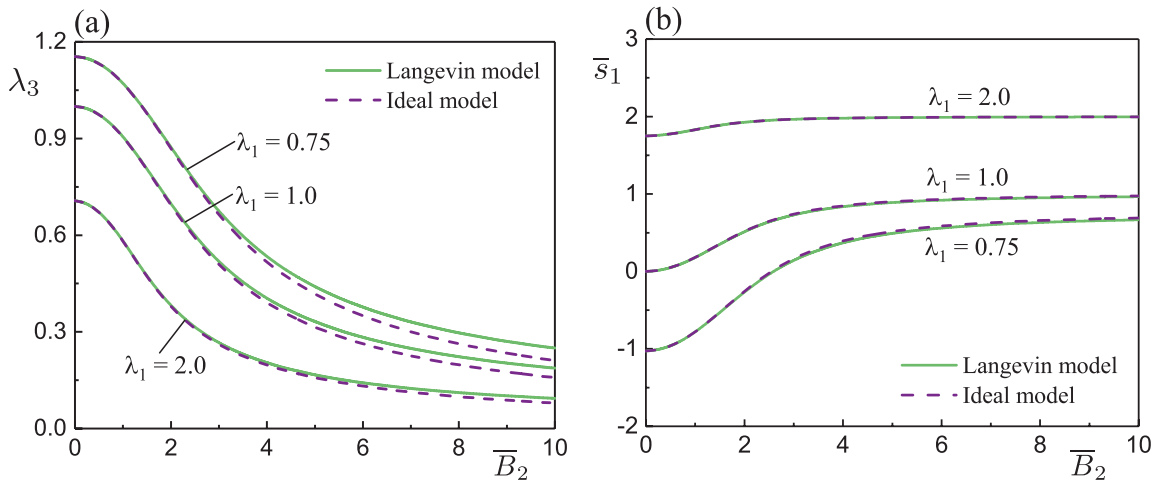

Figure 3: Uni-axial loading for three different values of pre-stretch $\lambda_1 = 0.75, 1.0, 2.0$: (a) response of the stretch ratio λ_3 versus the dimensionless magnetic induction field $\overline{B}_2$ from Eq. $(75)_2$; (b) response of the dimensionless nominal mechanical traction $\overline{s}_1$ versus $\overline{B}_2$ from Eq. $(75)_1$. Solid lines correspond to the ideal magneto-elastic model while dashed lines represent the saturation Langevin model.

For uni-axial loading, the magnetization responses of the two material models are essentially the same as those for plane-strain loading, as shown in Fig. 2(a). For three different values of pre-stretch $\lambda_1 = 0.75, 1.0, 2.0$, Fig. 3(a) and 3(b) display the effect of the magnetic induction field $\overline{B}_2$ on the stretch ratio λ_3 and the nominal mechanical traction $\overline{s}_1$, respectively, for the two material models. Again, we point out that the induced mechanical and magnetic field distributions are assumed to be uniform when solving the nonlinear static response, as explained previously, and that the material models (67) and (68) neglect pure material magnetostriction. We observe from Fig. 3(a) that the stretch ratio λ_3 decreases notably with increasing $\overline{B}_2$ *only* due to the magnetic traction induced by the external Maxwell stress. The stretch λ_3 for the ideal model is slightly lower than that predicted by the saturation Langevin model, because the saturation magnetization generates a smaller stretch λ_2 in the thickness direction. It is clear from Fig. 3(b) that the mechanical traction $\overline{s}_1$ increases gradually with $\overline{B}_2$. After $\overline{B}_2$ reaches a certain value, $\overline{s}_1$ remains unchanged. This is

because the in-plane elongation trend due to the compression in the x_3 direction counteracts the in-plane contraction tendency due to the external Maxwell stress in the x_1 direction. Furthermore, in the whole $\overline{B}_2$ range of interest, the mechanical tractions based on the two material models are almost identical, because the saturation magnetization does not alter the contraction trend in the x_1 direction and just affects the compression amount in the x_3 direction.

5.2. Bifurcation analysis

We now examine the critical values of stretch in the x_1 direction and of transverse magnetic induction field for which antisymmetric (see Fig. 1(d)) and symmetric (see Fig. 1(e)) modes of wrinkling instability appear.

For *plane-strain* loading, antisymmetric modes are identified by bifurcation equations (64) and (77) with $\lambda_1 = \lambda, \lambda_3 = 1$ for the two material models. The critical buckling fields of antisymmetric modes for *uni-axial* loading are calculated by solving bifurcation equations (64) and (77) together with nonlinear static response $(75)_2$. The corresponding critical fields of symmetric modes are calculated by using coth to replace tanh in Eqs. (64) and (77). The wrinkling criteria for thin- and thick-plate limits are obtained by evaluating Eqs. (65) and (66) or Eqs. (78) and (79) for the two material models.

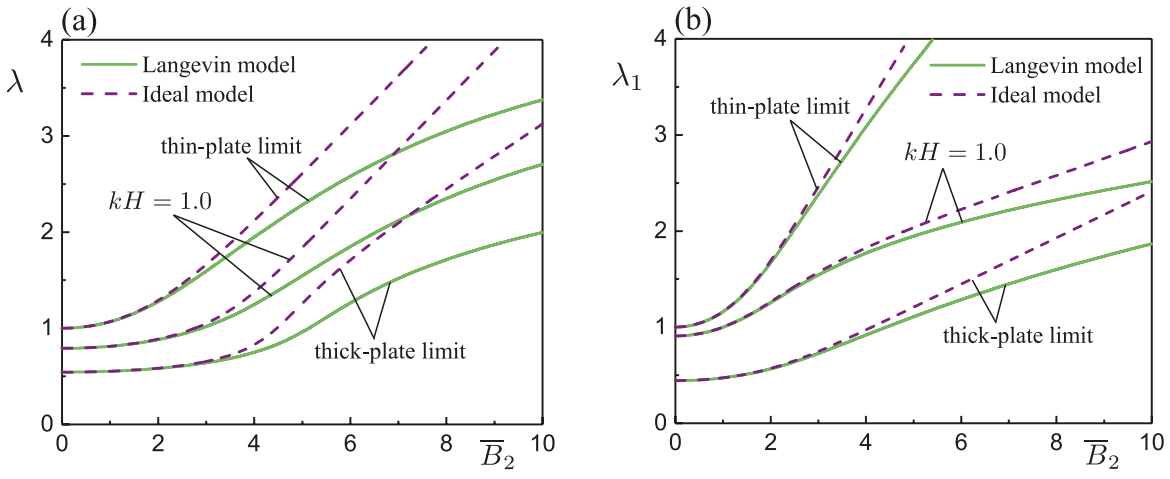

Figure 4: Bifurcation curves (or critical combinations of stretch ratio and dimensionless magnetic induction field) of antisymmetric wrinkling modes for the thin- and thick-plate limits and $kH = 1.0$: (a) plane-strain loading (λ versus $\overline{B}_2$); (b) uni-axial loading (λ_1 versus $\overline{B}_2$). Solid lines correspond to the ideal magneto-elastic model while dashed lines represent the saturation Langevin model.

For plane-strain loading and uni-axial loading, Fig. 4(a) and 4(b) illustrate the critical combinations of stretch ratio λ or λ_1 and dimensionless magnetic induction field $\overline{B}_2$ of antisymmetric wrinkling modes for the two material models. Specifically, Fig. 4 shows the

results corresponding to the thin- and thick-plate limits and a representative value of $kH = 1$. Since it is found that antisymmetric modes always occur first, Fig. 4 does not display the results for symmetric modes, which are addressed below.

We first focus on the results for the ideal magneto-elastic model in Fig. 4. In the absence of magnetic field ($\overline{B}_2 = 0$, purely elastic case), a thin plate with $kH \to 0$ is unstable for $\lambda < 1$ ($\lambda_1 < 1$) and is stable for any $\lambda > 1$ ($\lambda_1 > 1$) for plane-strain (uni-axial) loading. For both loading modes, a larger value of the parameter kH requires an increasing compression to induce instability. In the thick-plate limit $kH \to \infty$, we recover the well-known critical compression stretches for surface instability in the purely elastic case, namely $\lambda^{\rm cr} = 0.544$ and $\lambda_1^{\rm cr} = 0.444$ for plane-strain and uni-axial loading, respectively (Beatty and Pan, 1998). For a fixed non-zero $\overline{B}_2$, the variation trends of the critical stretch $\lambda^{\rm cr}$ or $\lambda_1^{\rm cr}$ with increasing kH are qualitatively the same as that for $\overline{B}_2 = 0$. Besides, the critical magnetic field $\overline{B}_2^{\rm cr}$, for a given stretch λ or λ_1, increases monotonically with kH, resulting in enhanced stability.

Furthermore, for a given kH, Fig. 4(a) shows that the critical stretch $\lambda^{\rm cr}$ exhibits a monotonous increase when $\overline{B}_2$ goes up, which means that the plate become more and more unstable and the magnetic field has a destabilizing effect. In particular, thin plates with $kH \to 0$ are unstable in tension ($\lambda^{\rm cr} > 1$) for non-zero $\overline{B}_2$, while the plate with $kH = 1$ has a wrinkling instability in tension for $\overline{B}_2 \gtrsim 2.8$. Similar phenomena are observed in Fig. 4(b) for uni-axial loading.

We now evaluate the effect of saturation magnetization on the stability. Fig. 4(a) shows that for plane-strain loading, the critical stretch $\lambda^{\rm cr}$ predicted by the saturation Langevin model coincides with that based on the ideal model for small and moderate values of $\overline{B}_2$, the range of which depends on kH. For example, the results based on the two material models are almost the same when $\overline{B}_2 \lesssim 3.0, 3.5, 4.0$ for $kH = 0, 1, \infty$, respectively. However, the presence of saturation magnetization reduces remarkably the critical stretch $\lambda^{\rm cr}$ for a large value of $\overline{B}_2$. These phenomena are also found in Fig. 4(b) for uni-axial loading. Nevertheless, compared with plane-strain loading, the effect of saturation magnetization on the critical fields is weaker for uni-axial loading because there is no constraint in the x_3 direction.

5.2.1. Critical stretch for a prescribed magnetic load

For a prescribed magnetic induction field, we first determine the critical stretch of the underlying deformed configuration for which antisymmetric and symmetric wrinkling modes

are induced. Specifically, for plane-strain (uni-axial) loading, Fig. 5(a) (Fig. 6(a)) displays the variation of the critical stretch $\lambda^{\rm cr}$ ($\lambda_1^{\rm cr}$) with kH for the neo-Hookean magnetization saturation SMA plates subject to three representative values of $\overline{B}_2 = 0, 2.5, 5.0$ ($\overline{B}_2 = 0, 2.5, 4.0$), wherein the antisymmetric and symmetric solutions are represented by the solid and dashed-dotted lines, respectively.

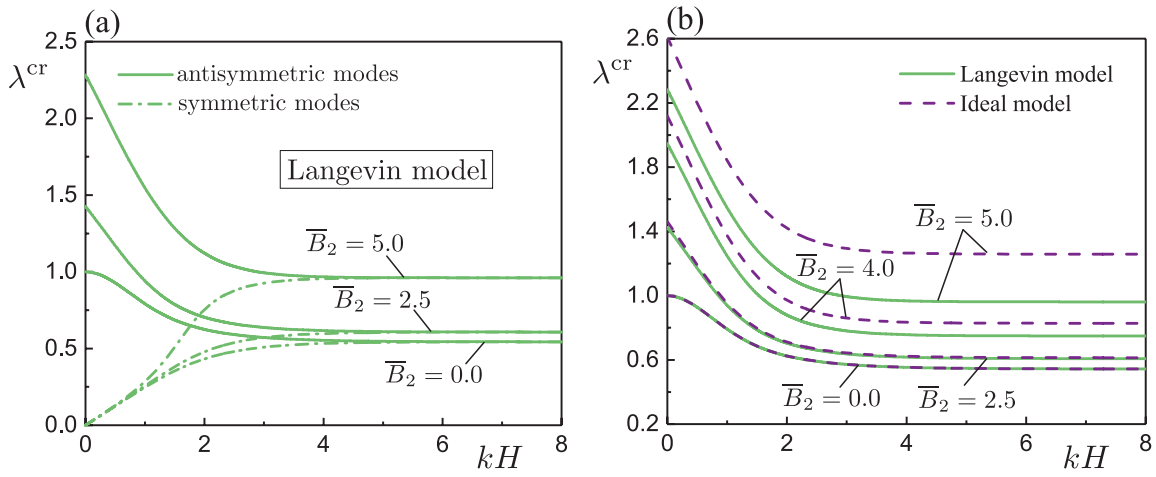

Figure 5: Plane-strain loading: (a) critical stretch $\lambda^{\rm cr}$ as a function of kH for antisymmetric (solid lines) and symmetric (dashed-dotted lines) modes of the neo-Hookean saturation Langevin plates subject to three prescribed values of $\overline{B}_2 = 0.0, 2.5, 5.0$; (b) $\lambda^{\rm cr}$ as a function of kH for antisymmetric modes of the neo-Hookean ideal (dashed lines) and saturation Langevin (solid lines) magneto-elastic plates subject to four fixed values of $\overline{B}_2 = 0.0, 2.5, 4.0, 5.0$.

We find from Figs. 5(a) and 6(a) that antisymmetric modes always occur before symmetric modes become possible for any value of kH. Therefore, to realize a symmetric buckling mode we must in principle suppress the appearance of the antisymmetric mode.

For a fixed $\overline{B}_2$, the critical stretch $\lambda^{\rm cr}$ (or $\lambda_1^{\rm cr}$) required to initiate the antisymmetric instability decreases monotonically with increasing kH, asymptotically approaching the surface instability of the thick-plate limit when $kH \to \infty$. However, the symmetric bifurcation curves exhibit an opposite trend. Thus, the stable range of combinations of λ (or λ_1) and kH is determined by the region above the solid line for a fixed $\overline{B}_2$. Moreover, the critical stretch $\lambda^{\rm cr}$ (or $\lambda_1^{\rm cr}$) for any value of kH is shifted upwards when raising $\overline{B}_2$, thus indicating that the SMA plate is destabilized by the application of an increasing magnetic field. In particular, for plane-strain loading with $\overline{B}_2 = 0, 2.5, 5.0$, the critical stretches $\lambda^{\rm cr}$ of a plate with $kH \to 0$ are 1.000, 1.426, 2.282, while those with $kH \to \infty$ are 0.544, 0.608, 0.961, respectively. For uni-axial loading with $\overline{B}_2 = 0, 2.5, 4.0$, the critical stretches $\lambda_1^{\rm cr}$ of the thin-plate limit are equal to 1.000, 2.016, 3.080, while those of the thick-plate limit are 0.444, 0.639, 0.918, respectively. The effect of small magnetic field on the stability is more

significant for uni-axial loading than for plane-strain loading.

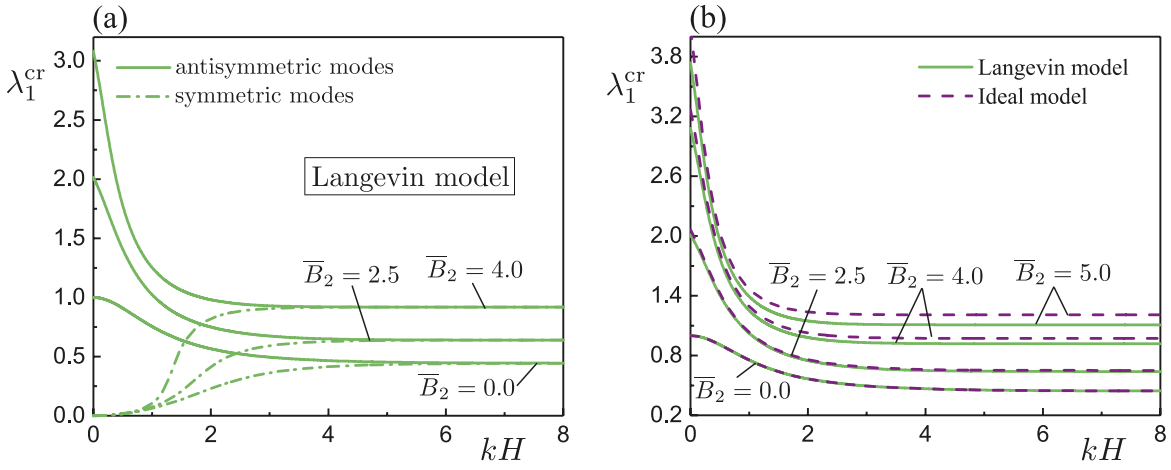

Figure 6: Uni-axial loading: (a) critical stretch λ_1^{cr} as a function of kH for anti-symmetric (solid lines) and symmetric (dashed-dotted lines) modes of the neo-Hookean saturation Langevin plates subject to three prescribed values of $\overline{B}_2 = 0.0, 2.5, 4.0$; (b) λ_1^{cr} as a function of kH for anti-symmetric modes of the neo-Hookean ideal (dashed lines) and saturation Langevin (solid lines) magneto-elastic plates subject to four fixed values of $\overline{B}_2 = 0.0, 2.5, 4.0, 5.0$.

For antisymmetric modes, Figs. 5(b) and 6(b) illustrate how the saturation magnetization affects the bifurcation curves (λ^{cr} versus kH and λ_1^{cr} versus kH) for plane-strain and uni-axial loading, respectively. We see that the bifurcation curves based on the two material models overlap in the entire range of kH for $\overline{B}_2 \leq 2.5$. This means that the critical stretch is hardly affected by the saturation magnetization for small to moderate values of the magnetic field. However, the saturation magnetization plays an important role in determining the critical stretch λ^{cr} or λ_1^{cr} for large values of $\overline{B}_2$: the figures show that it then stabilizes the SMA plate, and that its effect is much stronger for plane-strain loading than for uni-axial loading.

5.2.2. Critical magnetic induction field for a fixed pre-stretch

We now evaluate the effect of pre-stretch on the bifurcation curves ($\overline{B}_2^{cr}$ versus kH) of antisymmetric and symmetric wrinkling modes. For plane-strain (uni-axial) loading, Fig. 7(a) (Fig. 8(a)) shows the critical magnetic induction field $\overline{B}_2^{cr}$ as a function of kH for the neo-Hookean magnetization saturation SMA plates for four different levels of pre-stretch λ or $\lambda_1 = 0.8, 0.9, 1.0, 1.25$. Note that the solid and dashed-dotted lines denote the antisymmetric and symmetric solutions, respectively.

We observe from Figs. 7(a) and 8(a) that antisymmetric wrinkling modes are always triggered before the symmetric modes in the entire range of kH, which is analogous to what Figs. 5(a) and 6(a) show. As kH increases, the critical magnetic field $\overline{B}_2^{cr}$ for a given pre-stretch increases gradually for antisymmetric modes and decreases monotonically for

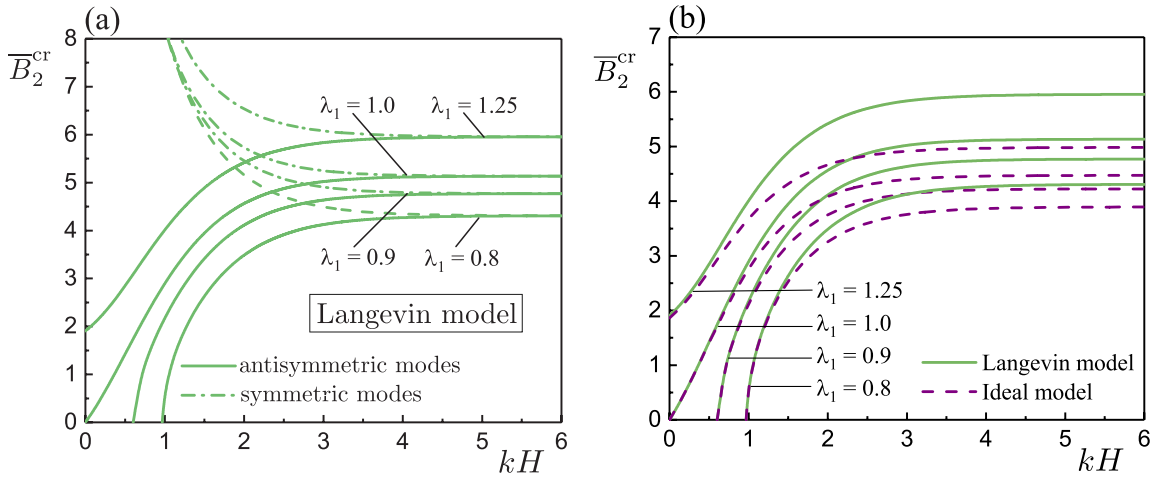

Figure 7: Plane-strain loading for four fixed values of pre-stretch $\lambda = 0.8, 0.9, 1.0, 1.25$: (a) critical magnetic induction field $\overline{B}_2^{\rm cr}$ as a function of kH for antisymmetric (solid lines) and symmetric (dashed-dotted lines) modes of the neo-Hookean saturation Langevin plates; (b) $\overline{B}_2^{\rm cr}$ as a function of kH for antisymmetric modes of the neo-Hookean ideal (dashed lines) and saturation Langevin (solid lines) magneto-elastic plates.

symmetric modes, both asymptotically tending to the surface instability of the thick-plate limit. The stable region of $\overline{B}_2$ and kH for a fixed pre-stretch is enclosed below the solid line for antisymmetric modes. Furthermore, an increase in the pre-stretch results in a larger value of $\overline{B}_2^{\rm cr}$ for a given kH. This means that increasing the pre-stretch enhances the stability of SMA plates.

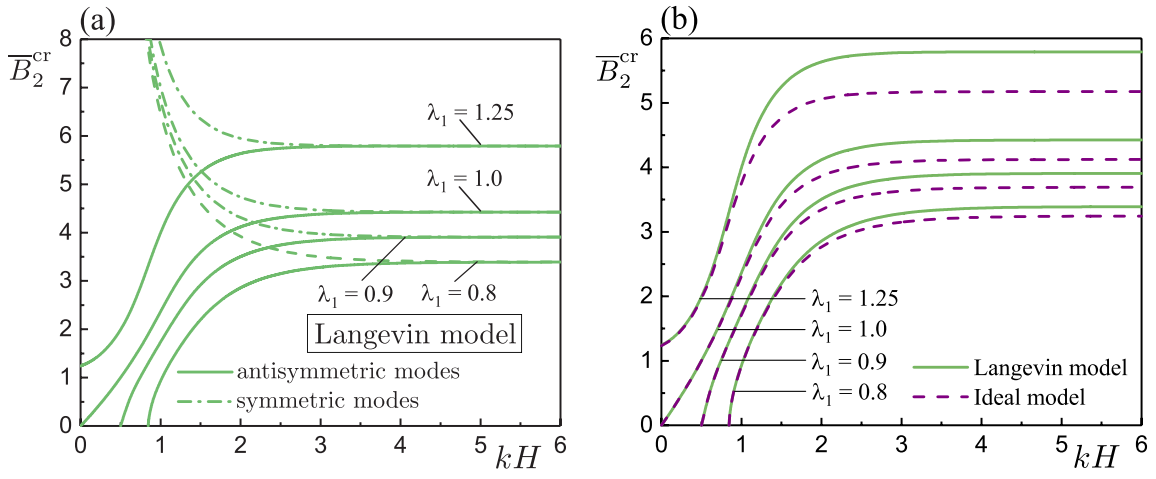

Figure 8: Uni-axial loading for four fixed values of pre-stretch $\lambda_1 = 0.8, 0.9, 1.0, 1.25$: (a) critical magnetic induction field $\overline{B}_2^{\rm cr}$ as a function of kH for antisymmetric (solid lines) and symmetric (dashed-dotted lines) modes of the neo-Hookean saturation Langevin plates; (b) $\overline{B}_2^{\rm cr}$ as a function of kH for antisymmetric modes of the neo-Hookean ideal (dashed lines) and saturation Langevin (solid lines) magneto-elastic plates.

Besides, we see from Figs. 7(a) and 8(a) that in the absence of pre-stretch (i.e., $\lambda = 1$ or $\lambda_1 = 1$), a thin plate ($kH \to 0$) buckles immediately when subject to an extremely small transverse magnetic field. By contrast, for a thin plate with a pre-stretch (say $\lambda = 1.25$ or $\lambda_1 = 1.25$), a non-zero magnetic induction field $\overline{B}_2^{\rm cr} \simeq 2.0$ (plane-strain loading) or $\overline{B}_2^{\rm cr} \simeq 1.25$

(uni-axial loading) is required to trigger the buckling instability. Interestingly, if an SMA plate with small values of kH is subject to a pre-compression (i.e., the pre-stretch is less than 1), the underlying configuration is unstable for any applied $\overline{B}_2$. For example, a plate with $\lambda = 0.8$ or $\lambda_1 = 0.8$ is unstable for $kH \lesssim 0.97$ under plane-strain loading and for $kH \lesssim 0.85$ under uni-axial loading. Physically, this means that plates with small values of kH do not support pre-compression even if there is no magnetic field.

For antisymmetric modes, the effect of saturation magnetization on the bifurcation curves ($\overline{B}_2^{\rm cr}$ versus kH) is highlighted in Figs. 7(b) and 8(b) for plane-strain and uni-axial loadings, respectively. We observe that for a given pre-stretch, the two material models predict an identical critical magnetic field $\overline{B}_2^{\rm cr}$ for small and moderate values of kH. For example, the bifurcation curves of a plate without pre-stretch ($\lambda = 1$ or $\lambda_1 = 1$) overlap for $kH \lesssim 1.0$ and $kH \lesssim 1.4$ under plane-strain and uni-axial loading, respectively. For a large value of kH with a fixed pre-stretch, the saturation Langevin model leads to a higher $\overline{B}_2^{\rm cr}$ compared with the prediction of the ideal magneto-elastic model. On the other hand, for a large value of kH, the predicted difference based on the two material models become larger and larger when increasing the pre-stretch.

5.2.3. Euler's buckling approximations

For the magneto-elastic coupling case, it is useful to establish thin-plate approximate equations (i.e., the Euler buckling solutions) of the antisymmetric wrinkling modes, as they always occurs first. The derivation procedure is provided in Appendix C in detail. We specialize the analysis to the neo-Hookean ideal magneto-elastic model (67) because its predicted bifurcation curves coincide with those based on the magnetization saturation model for small and moderate values of kH, as shown in Figs. 5-8.

For plane-strain loading, we find that the critical stretch is approximated as

$$\lambda^{\rm cr} = \lambda_0 + \left[\frac{1-\lambda_0^4}{2\left(1+\lambda_0^4\right)(1-\chi)}\right] kH - \left[\frac{2\lambda_0^3}{3\left(1+\lambda_0^4\right)} - \frac{\lambda_0^{12}+11\lambda_0^8-9\lambda_0^4-3}{8\lambda_0\left(1+\lambda_0^4\right)^3(1-\chi)^2}\right](kH)^2, \quad (80)$$

where

$$\lambda_0 = \sqrt{\frac{\chi^2\overline{B}_2^2}{2(1-\chi)} + \sqrt{\frac{\chi^4\overline{B}_2^4}{4(1-\chi)^2}+1}}. \quad (81)$$

Note that if there is no magnetic field ($\overline{B}_2 = 0$), then $\lambda_0 = 1$, the correction of order one vanishes, and $\lambda^{\rm cr} = 1 - (kH)^2/3$, in agreement with the classical Euler solution for the

buckling of a slender plate under plane-strain loading (Beatty and Pan, 1998). In Appendix C we also establish the quadratic expansions of the critical magnetic field and the corresponding expansions for the uni-axial loading mode.

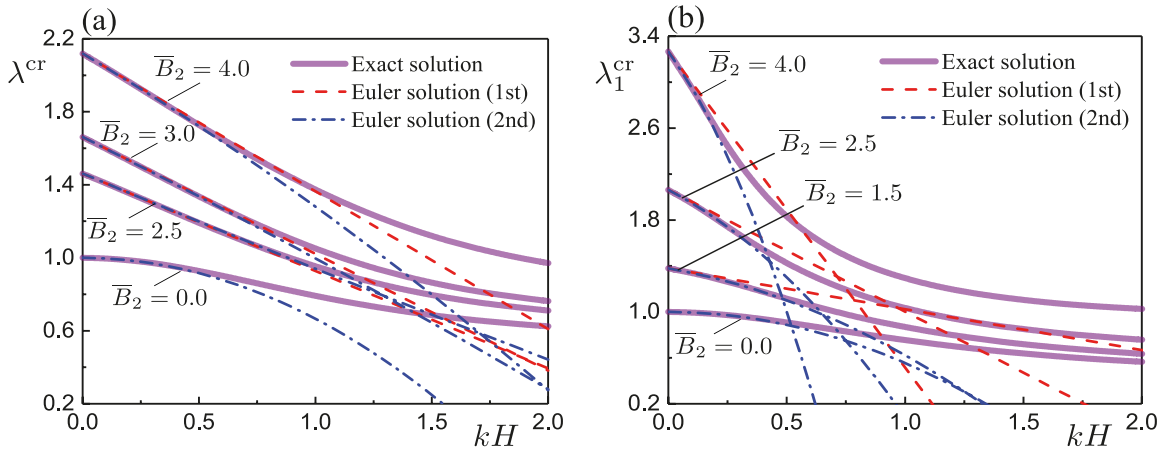

Figure 9: Critical stretch as a function of kH for antisymmetric modes of a neo-Hookean ideal magneto-elastic plate subject to different fixed values of $\overline{B}_2$: (a) plane-strain loading ($\lambda^{\rm cr}$ versus kH) with $\overline{B}_2 = 0.0, 2.5, 3.0, 4.0$; (b) uni-axial loading ($\lambda_1^{\rm cr}$ versus kH) with $\overline{B}_2 = 0.0, 1.5, 2.5, 4.0$. The solid lines, dashed lines, and dashed-dotted lines represent, respectively, the exact solutions, the first-order and second-order Euler buckling solutions.

Fig. 9 compares the critical stretch $\lambda^{\rm cr}$ or $\lambda_1^{\rm cr}$ versus kH based on the exact solutions to that calculated by the thin-plate buckling approximations. Fig. 10 illustrates the bifurcation curves of the critical magnetic induction field $\overline{B}_2^{\rm cr}$ versus kH obtained by the exact solutions and the Euler buckling solutions. The results for plane-strain loading are shown in Figs. 9(a) and 10(a) while those for uni-axial loading are depicted in Figs. 9(b) and 10(b). The solid, dashed, and dashed-dotted lines represent, respectively, the exact solutions, the first-order and second-order Euler solutions.

We see from Fig. 9 that in the absence of magnetic field ($\overline{B}_2 = 0$), the $\lambda^{\rm cr} - kH$ curve and the $\lambda_1^{\rm cr} - kH$ curve for the thin plate should be approximated quadratically, as in the purely elastic case (Beatty and Pan, 1998). For $\overline{B}_2 \neq 0$, the earliest correction for the stretch is of the first order in kH. For plane-strain loading, the first-order Euler solutions provide enough accuracy to approximate the exact solutions without having to resort to the second-order correction. However, for uni-axial loading, the linear approximations are not great and the quadratic corrections are required to approximate the exact bifurcation curves.

Fig. 10 shows that in the absence of pre-stretch ($\lambda = 1$ or $\lambda_1 = 1$), the first-order Euler buckling solutions can approximate well the $\overline{B}_2^{\rm cr} - kH$ curve for the thin plate under the two loading modes, as described by Kankanala and Triantafyllidis (2008). But for a pre-stretch

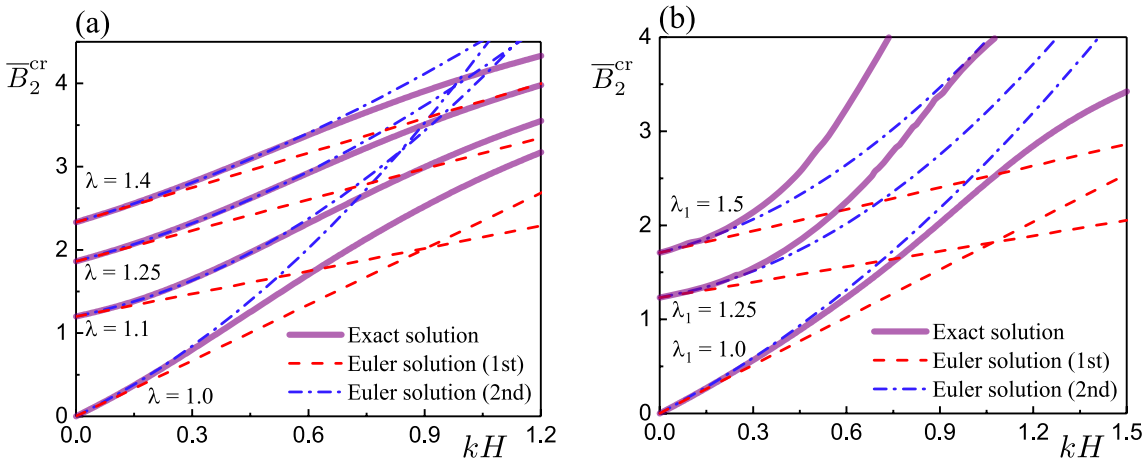

Figure 10: Critical magnetic induction field $\overline{B}_2^{\rm cr}$ as a function of kH for antisymmetric modes of a neo-Hookean ideal magneto-elastic plate subject to different fixed pre-stretch: (a) plane-strain loading with $\lambda = 1.0, 1.1, 1.25, 1.4$; (b) uni-axial loading with $\lambda_1 = 1.0, 1.25, 1.5$. The solid lines, dashed lines, and dashed-dotted lines represent, respectively, the exact solutions, the first-order and second-order Euler buckling solutions.

larger than 1, the $\overline{B}_2^{\rm cr} - kH$ curve should be approximated quadratically for small values of kH to enlarge the effective range of Euler's buckling solutions.

6. Conclusions

In the framework of nonlinear magneto-elasticity theory and its associated incremental formulation, we presented a comprehensive theoretical analysis of the wrinkling instability of SMA plates under the combined action of transverse magnetic field and in-plane mechanical loading. We discussed two loading modes (plane-strain loading and uni-axial loading) and two types of neo-Hookean magneto-elastic material models (ideal model and magnetization saturation model). Employing the Stroh formulation and the surface impedance method, we derived explicit bifurcation equations of symmetric and antisymmetric modes and obtained their corresponding thin- and thick-plate limits analytically. Finally, we conducted detailed calculations to demonstrate the dependence of the nonlinear static response and bifurcation diagrams on the loading mode, load amplitude, and saturation magnetization. Our main observations are summarized below:

(1) In contrast to the ideal model, introducting saturation magnetization results in a nonlinear magnetization response. Its effect on nonlinear mechanical response and critical buckling fields is more significant for plane-strain loading than for uni-axial loading.

(2) Antisymmetric wrinkling modes always appear before symmetric modes are expressed.

(3) Increasing the pre-compression and the magnetic field weakens the stability of SMA plates. However, the saturation magnetization effect strengthens their stability, especially for large pre-stretch or high magnetic field.

(4) The thin-plate approximate formulas agree well with the exact bifurcation curves for thin plates.

Note that we made the assumption of uniform magneto-mechanical biasing fields in this work to simplify the mathematical modelling of infinite SMA plates and to derive explicit analytical solutions. One factor that influences the uniformity of biasing fields is the shape and geometrical size of the SMA specimen. The mechanical and magnetic field distributions are usually non-uniform for ellipsoidal and cylindrical SMA specimens (see, for example, Martin et al. (2006); Rambausek and Keip (2018); Lefèvre et al. (2017, 2020)). In addition, the SMA plate slenderness may affect the magneto-mechanical field distributions. If the biasing fields are not uniform (i.e., they vary with spatial coordinates), then the Stroh formulation for wrinkling instabilities becomes a set of first-order differential equations with *variable* coefficients, which are difficult to solve analytically. Nonetheless, as shown by the work of Shuvalov et al. (2004) for example, the Stroh formalism is still useful and forms the basis of a robust numerical resolution with the surface impedance matrix method. Non-uniform biasing fields are beyond the scope of this preliminary paper and are worthy of further research.

Acknowledgement

This work was supported by the Government of Ireland Postdoctoral Fellowship from the Irish Research Council (No. GOIPD/2019/65). We thank the reviewers for raising insightful remarks on a previous version of the paper. We are grateful to Danas Kostas (CNRS, Ecole Polytechnique) for fruitful discussions.

Appendix A. Magneto-elastic moduli components

The three 3×3 real sub-matrices $\overline{\mathbf{N}}_i\,(i = 1, 2, 3)$ of the Stroh matrix $\overline{\mathbf{N}}$ in the Stroh formulation (33) are

$$\overline{\mathbf{N}}_1 = \begin{bmatrix} 0 & -1 + \overline{\tau}_{22}/\overline{c} & -\overline{d}/\overline{c} \\ -1 & 0 & 0 \\ -\overline{e}/\overline{g} & 0 & 0 \end{bmatrix}, \qquad \overline{\mathbf{N}}_2 = \begin{bmatrix} 1/\overline{c} & 0 & 0 \\ 0 & 0 & 0 \\ 0 & 0 & -1/\overline{g} \end{bmatrix},$$
$$\overline{\mathbf{N}}_3 = \begin{bmatrix} -2\left(\overline{b} + \overline{c} - \overline{\tau}_{22}\right) & 0 & 0 \\ 0 & -\overline{a} + \left(\overline{c} - \overline{\tau}_{22}\right)^2/\overline{c} & -\overline{d}\overline{\tau}_{22}/\overline{c} \\ 0 & -\overline{d}\overline{\tau}_{22}/\overline{c} & \overline{f} + \overline{d}^2/\overline{c} \end{bmatrix}, \tag{A.1}$$

where the dimensionless parameters $\overline{a} - \overline{g}$ and $\overline{\tau}_{22}$ are defined as

$$\begin{aligned} &\overline{a} = a/G, && \overline{b} = b/G, && \overline{c} = c/G, && \overline{\tau}_{22} = \tau_{22}/G, \\ &\overline{d} = d/\sqrt{G\mu_0}, && \overline{e} = e/\sqrt{G\mu_0}, && \overline{f} = f/\mu_0, && \overline{g} = g/\mu_0, \end{aligned} \tag{A.2}$$

with the magneto-elastic material parameters $a - g$ being

$$\begin{aligned} &a = c_{66} = \mathcal{A}_{01212} - \frac{\Gamma_{0211}^2}{K_{011}}, \quad c = c_{99} = \mathcal{A}_{02121} - \frac{\Gamma_{0211}^2}{K_{011}}, \quad d = e_{16} = -\frac{\Gamma_{0211}}{K_{011}}, \\ &e = e_{22} - e_{21} = \frac{\Gamma_{0112} - \Gamma_{0222}}{K_{022}}, \quad f = \mu_{11} = \frac{1}{K_{011}}, \quad g = \mu_{22} = \frac{1}{K_{022}}, \\ &2b = c_{11} + c_{22} - 2c_{12} - 2c_{69} + \frac{(e_{22} - e_{21})^2}{\mu_{22}} = 2\left(b_0 + \frac{\Gamma_{0211}^2}{K_{011}}\right), \\ &2b_0 = \mathcal{A}_{01111} + \mathcal{A}_{02222} - 2\mathcal{A}_{01122} - 2\mathcal{A}_{01221}, \end{aligned} \tag{A.3}$$

where $\boldsymbol{\mathcal{A}}_0$, $\boldsymbol{\Gamma}_0$ and $\mathbf{K}_0$ are the magneto-elastic moduli tensors. Note that we have used Eq. (31) and the relation $\mathcal{A}_{01221} + p = \mathcal{A}_{02121} - \tau_{22}$ from Eq. (23) to derive the Stroh matrix (A.1).

The total Cauchy stress tensor used in the Stroh matrix (A.1) is obtained from Eqs. (12) and $(13)_1$ as

$$\overline{\tau}_{22} = \overline{\tau}_{22}^{\star} = \overline{B}_2^2/2, \tag{A.4}$$

where $\overline{B}_2 = B_2/\sqrt{G\mu_0}$ is the dimensionless applied magnetic induction.

Using the incremental theory of magneto-elasticity (Otténio et al., 2008; Destrade and Ogden, 2011), we compute the instantaneous magneto-elastic moduli appearing in Eq. (A.3) for the applied bi-axial deformation λ_1, λ_3 and the transverse magnetic field B_2, as follows

$$
\begin{aligned}
&\mathcal{A}_{01212} = 2\lambda_1^2\left(\Omega_1 + \lambda_3^2\Omega_2 + B_2^2\Omega_6\right),\\
&\mathcal{A}_{02121} = 2\lambda_1^{-2}\lambda_3^{-2}\left\{\left(\Omega_1 + \lambda_3^2\Omega_2\right) + B_2^2\left[\lambda_1^2\lambda_3^2\Omega_5 + \left(2+\lambda_1^4\lambda_3^2\right)\Omega_6\right]\right\},\\
&b_0 = \left(\lambda_1^{-2}\lambda_3^{-2} + \lambda_1^2\right)\left(\Omega_1 + \lambda_3^2\Omega_2\right) + 2\left(\lambda_1^2 - \lambda_1^{-2}\lambda_3^{-2}\right)^2\left(\Omega_{11} + 2\lambda_3^2\Omega_{12} + \lambda_3^4\Omega_{22}\right)\\
&\quad + B_2^2\left\{4\left(\lambda_1^{-2}\lambda_3^{-2} - \lambda_1^2\right)\left[\left(\Omega_{15} + \lambda_3^2\Omega_{25}\right) + 2\lambda_1^{-2}\lambda_3^{-2}\left(\Omega_{16} + \lambda_3^2\Omega_{26}\right)\right]\right.\\
&\quad \left. + \Omega_5 + 2\left(3\lambda_1^{-2}\lambda_3^{-2} - \lambda_1^2\right)\Omega_6\right\} + 2B_2^4\left(\Omega_{55} + 4\lambda_1^{-2}\lambda_3^{-2}\Omega_{56} + 4\lambda_1^{-4}\lambda_3^{-4}\Omega_{66}\right),\\
&\Gamma_{0211} = 2B_2\left[\Omega_5 + \left(\lambda_1^2 + \lambda_1^{-2}\lambda_3^{-2}\right)\Omega_6\right],\\
&\Gamma_{0112} - \Gamma_{0222} = 4B_2\left\{\left(\lambda_1^4\lambda_3^2 - 1\right)\left[\left(\Omega_{14} + \lambda_3^2\Omega_{24}\right) + \lambda_1^{-2}\lambda_3^{-2}\left(\Omega_{15} + \lambda_3^2\Omega_{25}\right)\right.\right.\\
&\quad \left. + \lambda_1^{-4}\lambda_3^{-4}\left(\Omega_{16} + \lambda_3^2\Omega_{26}\right)\right] - \Omega_5 - 2\lambda_1^{-2}\lambda_3^{-2}\Omega_6\\
&\quad \left. - B_2^2\left(\lambda_1^2\lambda_3^2\Omega_{45} + 2\Omega_{46} + \Omega_{55} + 3\lambda_1^{-2}\lambda_3^{-2}\Omega_{56} + 2\lambda_1^{-4}\lambda_3^{-4}\Omega_{66}\right)\right\},\\
&K_{011} = 2\left(\lambda_1^{-2}\Omega_4 + \Omega_5 + \lambda_1^2\Omega_6\right),\\
&K_{022} = 2\left(\lambda_1^2\lambda_3^2\Omega_4 + \Omega_5 + \lambda_1^{-2}\lambda_3^{-2}\Omega_6\right) + 4B_2^2\left(\lambda_1^4\lambda_3^4\Omega_{44} + 2\lambda_1^2\lambda_3^2\Omega_{45}\right.\\
&\quad \left. + 2\Omega_{46} + \Omega_{55} + 2\lambda_1^{-2}\lambda_3^{-2}\Omega_{56} + \lambda_1^{-4}\lambda_3^{-4}\Omega_{66}\right).
\end{aligned}
\tag{A.5}
$$

After obtaining the eigenvalues q_j and eigenvectors $\overline{\boldsymbol{\eta}}^{(j)}$, the generalized displacement and traction vectors at the faces $x_2 = \pm h$ are expressed, according to Eq. (36), as

$$
\begin{bmatrix} \overline{\mathbf{U}}\,(kh) \\ \overline{\mathbf{U}}\,(-kh) \end{bmatrix} = \begin{bmatrix}
\overline{\eta}_1^{(1)}E_1^+ & \overline{\eta}_1^{(2)}E_2^+ & \overline{\eta}_1^{(3)}E_3^+ & \overline{\eta}_1^{(4)}E_1^- & \overline{\eta}_1^{(5)}E_2^- & \overline{\eta}_1^{(6)}E_3^- \\
\overline{\eta}_2^{(1)}E_1^+ & \overline{\eta}_2^{(2)}E_2^+ & \overline{\eta}_2^{(3)}E_3^+ & \overline{\eta}_2^{(4)}E_1^- & \overline{\eta}_2^{(5)}E_2^- & \overline{\eta}_2^{(6)}E_3^- \\
\overline{\eta}_3^{(1)}E_1^+ & \overline{\eta}_3^{(2)}E_2^+ & \overline{\eta}_3^{(3)}E_3^+ & \overline{\eta}_3^{(4)}E_1^- & \overline{\eta}_3^{(5)}E_2^- & \overline{\eta}_3^{(6)}E_3^- \\
\overline{\eta}_1^{(1)}E_1^- & \overline{\eta}_1^{(2)}E_2^- & \overline{\eta}_1^{(3)}E_3^- & \overline{\eta}_1^{(4)}E_1^+ & \overline{\eta}_1^{(5)}E_2^+ & \overline{\eta}_1^{(6)}E_3^+ \\
\overline{\eta}_2^{(1)}E_1^- & \overline{\eta}_2^{(2)}E_2^- & \overline{\eta}_2^{(3)}E_3^- & \overline{\eta}_2^{(4)}E_1^+ & \overline{\eta}_2^{(5)}E_2^+ & \overline{\eta}_2^{(6)}E_3^+ \\
\overline{\eta}_3^{(1)}E_1^- & \overline{\eta}_3^{(2)}E_2^- & \overline{\eta}_3^{(3)}E_3^- & \overline{\eta}_3^{(4)}E_1^+ & \overline{\eta}_3^{(5)}E_2^+ & \overline{\eta}_3^{(6)}E_3^+
\end{bmatrix}
\begin{bmatrix} A_1 \\ A_2 \\ A_3 \\ A_4 \\ A_5 \\ A_6 \end{bmatrix},
\tag{A.6}
$$

and

$$\begin{bmatrix} \overline{\mathbf{S}}\left(kh\right) \\ \overline{\mathbf{S}}\left(-kh\right) \end{bmatrix} = \begin{bmatrix} \overline{\eta}_4^{(1)}E_1^+ & \overline{\eta}_4^{(2)}E_2^+ & \overline{\eta}_4^{(3)}E_3^+ & \overline{\eta}_4^{(4)}E_1^- & \overline{\eta}_4^{(5)}E_2^- & \overline{\eta}_4^{(6)}E_3^- \\ \overline{\eta}_5^{(1)}E_1^+ & \overline{\eta}_5^{(2)}E_2^+ & \overline{\eta}_5^{(3)}E_3^+ & \overline{\eta}_5^{(4)}E_1^- & \overline{\eta}_5^{(5)}E_2^- & \overline{\eta}_5^{(6)}E_3^- \\ \overline{\eta}_6^{(1)}E_1^+ & \overline{\eta}_6^{(2)}E_2^+ & \overline{\eta}_6^{(3)}E_3^+ & \overline{\eta}_6^{(4)}E_1^- & \overline{\eta}_6^{(5)}E_2^- & \overline{\eta}_6^{(6)}E_3^- \\ \overline{\eta}_4^{(1)}E_1^- & \overline{\eta}_4^{(2)}E_2^- & \overline{\eta}_4^{(3)}E_3^- & \overline{\eta}_4^{(4)}E_1^+ & \overline{\eta}_4^{(5)}E_2^+ & \overline{\eta}_4^{(6)}E_3^+ \\ \overline{\eta}_5^{(1)}E_1^- & \overline{\eta}_5^{(2)}E_2^- & \overline{\eta}_5^{(3)}E_3^- & \overline{\eta}_5^{(4)}E_1^+ & \overline{\eta}_5^{(5)}E_2^+ & \overline{\eta}_5^{(6)}E_3^+ \\ \overline{\eta}_6^{(1)}E_1^- & \overline{\eta}_6^{(2)}E_2^- & \overline{\eta}_6^{(3)}E_3^- & \overline{\eta}_6^{(4)}E_1^+ & \overline{\eta}_6^{(5)}E_2^+ & \overline{\eta}_6^{(6)}E_3^+ \end{bmatrix} \begin{bmatrix} A_1 \\ A_2 \\ A_3 \\ A_4 \\ A_5 \\ A_6 \end{bmatrix}, \tag{A.7}$$

where $E_j^{\pm} = \mathrm{e}^{\pm \mathrm{i}q_j kh}\,(j = 1, \ldots, 6)$. Thus, we note from Eq. (41) that $E_j^{\pm} = \mathrm{e}^{\mp p_j kh}$ for $j = 1, 2, 3$ since $q_j = \mathrm{i}p_j\,(j = 1, 2, 3)$, and that $E_{j+3}^{\pm} = E_j^{\mp}$ for $j = 1, 2, 3$ since $q_{j+3} = -q_j\,(j = 1, 2, 3)$.

Appendix B. Bifurcation equation of surface instability based on the surface impedance method

Assume that the SMA half-space in the reference and current configurations occupies the region $X_2 \geq 0$ and $x_2 \geq 0$, respectively. To satisfy the decay condition at $x_2 \to +\infty$ in the half-space, we only keep the eigenvalues in Eq. (36) with positive imaginary parts. Thus, we take the three eigenvalues q_1, q_2, q_3 according to Eqs. (41) and (42). The general solution to the Stroh formulation (33) is written as

$$\overline{\boldsymbol{\eta}}\left(kx_2\right) = \begin{bmatrix} \overline{\mathbf{U}}\left(kx_2\right) \\ \overline{\mathbf{S}}\left(kx_2\right) \end{bmatrix} = \sum_{j=1}^{3} A_j \overline{\boldsymbol{\eta}}^{(j)} \mathrm{e}^{\mathrm{i}q_j kx_2} = \sum_{j=1}^{3} A_j \overline{\boldsymbol{\eta}}^{(j)} \mathrm{e}^{-p_j kx_2}, \tag{B.1}$$

where $q_j = \mathrm{i}p_j\,(j = 1, 2, 3)$ with $p_j > 0$. In matrix form, Eq. (B.1) is expressed as

$$\overline{\boldsymbol{\eta}}\left(kx_2\right) = \begin{bmatrix} \mathbf{P}_1 \\ \mathbf{P}_2 \end{bmatrix} \begin{bmatrix} \mathrm{e}^{-p_1 kx_2} & 0 & 0 \\ 0 & \mathrm{e}^{-p_2 kx_2} & 0 \\ 0 & 0 & \mathrm{e}^{-p_3 kx_2} \end{bmatrix} \begin{bmatrix} A_1 \\ A_2 \\ A_3 \end{bmatrix}, \tag{B.2}$$

where

$$\mathbf{P}_1 = \begin{bmatrix} \overline{\eta}_1^{(1)} & \overline{\eta}_1^{(2)} & \overline{\eta}_1^{(3)} \\ \overline{\eta}_2^{(1)} & \overline{\eta}_2^{(2)} & \overline{\eta}_2^{(3)} \\ \overline{\eta}_3^{(1)} & \overline{\eta}_3^{(2)} & \overline{\eta}_3^{(3)} \end{bmatrix}, \qquad \mathbf{P}_2 = \begin{bmatrix} \overline{\eta}_4^{(1)} & \overline{\eta}_4^{(2)} & \overline{\eta}_4^{(3)} \\ \overline{\eta}_5^{(1)} & \overline{\eta}_5^{(2)} & \overline{\eta}_5^{(3)} \\ \overline{\eta}_6^{(1)} & \overline{\eta}_6^{(2)} & \overline{\eta}_6^{(3)} \end{bmatrix}, \tag{B.3}$$

Setting $x_2 = 0$, we obtain from Eqs. (B.1) and (B.2) that

$$\overline{\mathbf{S}}\,(0) = \mathrm{i}\overline{\mathbf{Z}}\overline{\mathbf{U}}\,(0)\,, \tag{B.4}$$

where $\overline{\mathbf{Z}} = -\mathrm{i}\mathbf{P}_2\mathbf{P}_1^{-1}$ is the surface impedance matrix of the half-space, through which the generalized traction and displacement vectors at the face $x_2 = 0$ are connected.

In view of Eqs. (55) and (56), the surface impedance matrix exterior to the material is

$$\overline{\mathbf{Z}}^{\star} = \begin{bmatrix} 0 & \mathrm{i}\overline{B}_2^2/2 & \mathrm{i}\overline{B}_2 \\ -\mathrm{i}\overline{B}_2^2/2 & \overline{B}_2^2 & \overline{B}_2 \\ -\mathrm{i}\overline{B}_2 & \overline{B}_2 & 1 \end{bmatrix}, \tag{B.5}$$

which, at the face $x_2 = 0$, satisfies

$$\overline{\mathbf{S}}\,(0) = \mathrm{i}\overline{\mathbf{Z}}^{\star}\overline{\mathbf{U}}\,(0)\,. \tag{B.6}$$

From Eqs. (B.4) and (B.6), we get the bifurcation equation governing the surface wrinkling instability, as

$$\det\left(\overline{\mathbf{Z}} - \overline{\mathbf{Z}}^{\star}\right) = 0. \tag{B.7}$$

Substituting Eqs. (A.4), (38), $(42)_{1,2}$, $(43)_{1,2,3}$ and (B.5) into Eq. (B.7) and with the help of Mathematica, we obtain the explicit bifurcation equation for the surface wrinkles as

$$\begin{aligned} \left[1+\beta\left(\lambda_3^2-1\right)\right]\left(1+2\overline{F}_5 p_3\right)\left[\left(\lambda_1^2\lambda_3\right)^3+\left(\lambda_1^2\lambda_3\right)^2+3\lambda_1^2\lambda_3-1\right] \\ -\overline{B}_2^2\left(1-2\overline{F}_5\right)^2\lambda_1^2\lambda_3^2\left(\lambda_1^2\lambda_3+1\right)=0, \end{aligned} \tag{B.8}$$

which is the same as Eq. (65).

Appendix C. Thin-plate buckling approximations

For the neo-Hookean ideal magneto-elastic model (67), this appendix makes use of the exact bifurcation equation (77) to establish thin-plate approximations to antisymmetric wrinkling modes, which always occur first.

Appendix C.1. Plane-strain loading

For plane-strain loading, the exact bifurcation equation (77) becomes

$$[1-\chi+\tanh(kh)]\left[\left(1+\lambda^4\right)^2\tanh(kh)-4\lambda^2\tanh\left(\lambda^2 kh\right)\right] = \overline{B}_2^2\chi^2\lambda^2\left(\lambda^4-1\right)\tanh(kh), \quad \text{(C.1)}$$

where $kh=\lambda^{-1}kH$. At the zero-th order in kH, the thin-plate equation (79) gives

$$\overline{B}_2^2=\chi^{-2}(1-\chi)\left(\lambda^2-\lambda^{-2}\right). \quad \text{(C.2)}$$

Appendix C.1.1. Critical stretch

For a fixed magnetic induction field $\overline{B}_2$, we first derive the approximations of the critical stretch $\lambda^{\rm cr}$. In this case, we denote the root of Eq. (C.2) as λ_0. In the thin-plate limit ($kH\to 0$), we may expand the tanh functions in Eq. (C.1) in power series as follows:

$$\tanh(kh)\approx\lambda^{-1}kH-\left(\lambda^{-1}kH\right)^3/3, \qquad \tanh\left(\lambda^2 kh\right)\approx\lambda kH-(\lambda kH)^3/3. \quad \text{(C.3)}$$

Inserting Eq. (C.3) into Eq. (C.1) and retaining only terms of first order in kH, we obtain

$$(1-\lambda^2)(1+\lambda^2)kH+\lambda\left[(1-\chi)(1-\lambda^2)(1+\lambda^2)+\overline{B}_2^2\chi^2\lambda^2\right]=0. \quad \text{(C.4)}$$

As expected, when $kH=0$, λ is equal to λ_0. Hence, substituting the first-order expansion $\lambda^{\rm cr}=\lambda_0+\varepsilon_1 kH$ in Eq. (C.4) and retaining terms to the first order in kH, we find the equation governing ε_1 as

$$1-\lambda_0^4+\varepsilon_1\left[(1-\chi)(5-9\lambda_0^4)+7\overline{B}_2^2\chi^2\lambda_0^2\right]=0. \quad \text{(C.5)}$$

Using Eq. (C.2) in Eq. (C.5), we thus obtain the first-order correction of the critical stretch

$$\lambda^{\mathrm{cr}} = \lambda_0 + \frac{1-\lambda_0^4}{2\left(1+\lambda_0^4\right)(1-\chi)}kH. \tag{C.6}$$

Similarly, we insert the power series expansion (C.3) into Eq. (C.1) and retain only terms of second order in kH. Then, we introduce the second-order expansion of stretch $\lambda^{\mathrm{cr}} = \lambda_0 + \varepsilon_1 kH + \varepsilon_2 (kH)^2$ in the resultant equation, keep terms to the second order in kH, and thereby get the second-order correction of the critical stretch

$$\lambda^{\mathrm{cr}} = \lambda_0 + \frac{1-\lambda_0^4}{2\left(1+\lambda_0^4\right)(1-\chi)}kH + \varepsilon_2 (kH)^2, \tag{C.7}$$

where

$$\varepsilon_2 = -\frac{2\lambda_0^3}{3\left(1+\lambda_0^4\right)} + \frac{\lambda_0^{12}+11\lambda_0^8-9\lambda_0^4-3}{8\lambda_0\left(1+\lambda_0^4\right)^3(1-\chi)^2}. \tag{C.8}$$

When $\overline{B}_2 = 0$, we have $\lambda_0 = 1$ and from Eq. (C.7) the first correction for stretch is of order two: $\lambda^{\mathrm{cr}} = 1 - (kH)^2/3$. This is equivalent to the classical Euler solution for the buckling of a slender or a thin plate under plane-strain loading in the purely elastic case (Beatty and Pan, 1998).

Appendix C.1.2. Critical magnetic induction field

Next, we derive the approximations of the critical magnetic field $\overline{B}_2^{\mathrm{cr}}$ for a given pre-stretch λ. In this case, the root of Eq. (C.2) is represented by $\overline{B}_{20}$. Analogous to the derivations of the critical stretch described in Appendix C.1.1, we obtain

$$\overline{B}_2^{\mathrm{cr}} = \overline{B}_{20}\left[1 + \frac{1}{2\lambda(1-\chi)}kH\right] \tag{C.9}$$

for the first-order correction, and

$$\overline{B}_2^{\mathrm{cr}} = \overline{B}_{20}\left[1 + \frac{1}{2\lambda(1-\chi)}kH + \gamma_2(kH)^2\right], \qquad \gamma_2 = \frac{3+\lambda^4\left[13+16\chi(\chi-2)\right]}{24\lambda^2\left(\lambda^4-1\right)(1-\chi)^2} \tag{C.10}$$

for the second-order correction.

However, in the special case where there is no pre-stretch ($\lambda = 1$), we see that $\overline{B}_{20} = 0$ from Eq. (C.2). In that case, Eqs. (C.9) and (C.10) give $\overline{B}_2^{\mathrm{cr}} \equiv 0$, which is independent of kH and unphysical. That case thus requires a separate treatment. Expanding the bifurcation

equation (C.1) in power series in kH, keeping terms up to the third order in kH, and setting $\lambda = 1$, we have

$$-4(kH)^3 + \left[4(\chi-1) - \overline{B}_2^2\chi^2\right](kH)^2 + 3\overline{B}_2^2\chi^2 = 0. \tag{C.11}$$

Then, we introduce the first-order expansion of the critical magnetic field $\overline{B}_2^{\rm cr} = \gamma_{10}kH$ in Eq. (C.11), keep terms to the second order in kH, and obtain the first-order correction as

$$\overline{B}_2^{\rm cr} = \frac{2\sqrt{1-\chi}}{\sqrt{3}\chi}kH. \tag{C.12}$$

Further, the second-order correction of the critical magnetic field is found as

$$\overline{B}_2^{\rm cr} = \frac{2\sqrt{1-\chi}}{\sqrt{3}\chi}kH + \frac{1}{\chi\sqrt{3\,(1-\chi)}}(kH)^2. \tag{C.13}$$

Note that the thin-plate buckling approximation (C.13) of $\overline{B}_2^{\rm cr}$ agrees with the classical asymptotic formula obtained by Pao and Yeh (1973) (see their Eq. (8.13) and let the Poisson ratio in their formula tend to 1/2 for incompressible materials).

Appendix C.2. Uni-axial loading

For uni-axial loading, the exact bifurcation equation for antisymmetric wrinkles is governed by Eq. (77), which is reproduced here, as

$$\begin{aligned}[1-\chi+\tanh(kh)]\left[\left(1+\lambda_1^4\lambda_3^2\right)^2\tanh(kh) - 4\lambda_1^2\lambda_3\tanh\left(\lambda_1^2\lambda_3 kh\right)\right] \\ = \overline{B}_2^2\chi^2\lambda_1^2\lambda_3^2\left(\lambda_1^4\lambda_3^2-1\right)\tanh(kh),\end{aligned} \tag{C.14}$$

where $kh = \lambda_1^{-1}\lambda_3^{-1}kH$, and from Eq. $(75)_2$ we obtain the nonlinear mechanical response (determining λ_3) for the ideal magneto-elastic model as

$$\lambda_3^2 - \lambda_1^{-2}\lambda_3^{-2} + \chi\overline{B}_2^2 = 0. \tag{C.15}$$

At the zero-th order in kH, the thin-plate equation (79) gives

$$\overline{B}_2^2 = \chi^{-2}(1-\chi)\left(\lambda_1^2 - \lambda_1^{-2}\lambda_3^{-2}\right). \tag{C.16}$$

Appendix C.2.1. Critical stretch

First, the approximations of the critical stretches $\lambda_1^{\rm cr}$ and $\lambda_3^{\rm cr}$ are derived according to Eqs. (C.14) and (C.15) for a fixed $\overline{B}_2$. The root of the zero-order equations (C.15) and (C.16) is denoted by λ_{10} and λ_{30}. For $kH \to 0$, we expand Eq. (C.14) up to the first order in kH, as

$$(1-\lambda_1^4\lambda_3^2)kH + \lambda_1\lambda_3\left[(1-\chi)(1-\lambda_1^4\lambda_3^2) + \overline{B}_2^2\chi^2\lambda_1^2\lambda_3^2\right] = 0. \tag{C.17}$$

We then introduce the first-order corrections $\lambda_1^{\rm cr} = \lambda_{10} + \varepsilon_1 kH$ and $\lambda_3^{\rm cr} = \lambda_{30} + \varepsilon_2 kH$ into Eqs. (C.15) and (C.17), and retain terms to the first order in kH. The resultant zero-order terms satisfy the zero-order thin-plate equations (C.15) and (C.16), while the first-order terms constitute a set of two linear algebraic equations for ε_1 and ε_2, which are solved as

$$\varepsilon_1 = \frac{\left(1-\lambda_{10}^4\lambda_{30}^2\right)\left(1+\lambda_{10}^2\lambda_{30}^4\right)}{2\lambda_{10}^2\lambda_{30}^3\left(\lambda_{10}^2+\lambda_{30}^2+\lambda_{10}^4\lambda_{30}^4\right)(1-\chi)}, \qquad \varepsilon_2 = -\frac{\lambda_{30}}{\lambda_{10}\left(1+\lambda_{10}^2\lambda_{30}^4\right)}\varepsilon_1. \tag{C.18}$$

The next order in kH is order two. With similar manipulations of Eqs. (C.14) and (C.15), we find the second-order correction of the critical stretches, as

$$\lambda_1^{\rm cr} = \lambda_{10} + \varepsilon_1 kH + \varepsilon_3 (kH)^2, \qquad \lambda_3^{\rm cr} = \lambda_{30} + \varepsilon_2 kH + \varepsilon_4 (kH)^2, \tag{C.19}$$

where ε_1 and ε_2 are determined by Eq. (C.18), and

$$[\varepsilon_3,\, \varepsilon_4]^{\rm T} = 2\mathbf{Q}_1^{-1}\,[t_1,\, t_2]^{\rm T}\,, \tag{C.20}$$

in which we have

$$\begin{aligned}
\mathbf{Q}_1 =& \begin{pmatrix} 9\lambda_{10}^4\lambda_{30}^5\left(1+\lambda_{10}^4\lambda_{30}^2\right)(\chi-1) & 9\lambda_{10}^5\lambda_{30}^4(\chi-1) \\ \lambda_{10}^{-1} & \lambda_{30}^{-1}\left(1+\lambda_{10}^2\lambda_{30}^4\right) \end{pmatrix}, \\
t_1 =& 12\lambda_{10}^7\lambda_{30}^5(1-\chi) + \frac{9k_1\left(1-\lambda_{10}^4\lambda_{30}^2\right)}{4\lambda_{10}\lambda_{30}\left(\lambda_{10}^2+\lambda_{30}^2+\lambda_{10}^4\lambda_{30}^4\right)^2(1-\chi)}, \\
t_2 =& \frac{\left(1-\lambda_{10}^4\lambda_{30}^2\right)^2\left(2+\lambda_{10}^2\lambda_{30}^4+3\lambda_{10}^4\lambda_{30}^8\right)}{4\lambda_{10}^6\lambda_{30}^6\left(\lambda_{10}^2+\lambda_{30}^2+\lambda_{10}^4\lambda_{30}^4\right)^2(1-\chi)^2}, \\
k_1 =& \lambda_{10}^4\lambda_{30}^2\left[\lambda_{10}^2\lambda_{30}^4\left(14+\lambda_{10}^6\lambda_{30}^6\right)+4\lambda_{10}^4\lambda_{30}^6\left(\lambda_{10}^2+3\lambda_{30}^2\right)\right. \\
& \left.+3\left(1+\lambda_{30}^6+\lambda_{10}^4\lambda_{30}^2\right)\right] - 2\left(1+\lambda_{10}^2\lambda_{30}^4\right).
\end{aligned} \tag{C.21}$$

Again we verify that for $\overline{B}_2 = 0$, we have $\lambda_{10} = \lambda_{30} = 1$ and from Eqs. (C.18)-(C.21) we recover the purely elastic result: $\lambda_1^{\rm cr} = 1 - 4(kH)^2/9$ and $\lambda_3^{\rm cr} = 1 + 2(kH)^2/9$. This is the classical Euler solution for the buckling of a slender or a thin plate under uni-axial loading (Beatty and Pan, 1998).

Appendix C.2.2. Critical magnetic induction field

We now derive the approximations of the critical magnetic field $\overline{B}_2^{\rm cr}$ for a given pre-stretch λ_1. We call the root of Eqs. (C.15) and (C.16) as $\overline{B}_{20}$ and λ_{30}. The derivation is essentially the same as the one of the critical stretch given in Appendix C.2.1. Hence, we get the first-order corrections

$$\overline{B}_2^{\rm cr} = \overline{B}_{20} + \gamma_1 kH, \qquad \lambda_3^{\rm cr} = \lambda_{30} + \gamma_2 kH, \tag{C.22}$$

with

$$\begin{aligned}
\gamma_1 &= \frac{\left(1-\lambda_1^4\lambda_{30}^2\right)\left(2\lambda_{30}^2 + \chi\overline{B}_{20}^2\right)}{\chi\overline{B}_{20}\lambda_1\lambda_{30}\left\{5\left(1-\chi\right) + \lambda_1^2\lambda_{30}^2\left[7\lambda_1^2\left(\chi-1\right) + \chi\left(5\chi\overline{B}_{20}^2 - 4\lambda_{30}^2\right)\right]\right\}}, \\
\gamma_2 &= \frac{\lambda_1^4\lambda_{30}^2 - 1}{\lambda_1\left\{5\left(1-\chi\right) + \lambda_1^2\lambda_{30}^2\left[7\lambda_1^2\left(\chi-1\right) + \chi\left(5\chi\overline{B}_{20}^2 - 4\lambda_{30}^2\right)\right]\right\}},
\end{aligned} \tag{C.23}$$

and the second-order corrections

$$\overline{B}_2^{\rm cr} = \overline{B}_{20} + \gamma_1 kH + \gamma_3 (kH)^2, \qquad \lambda_3^{\rm cr} = \lambda_{30} + \gamma_2 kH + \gamma_4 (kH)^2, \tag{C.24}$$

with

$$\left[\gamma_3,\, \gamma_4\right]^{\rm T} = -\mathbf{Q}_2^{-1}\left[t_3,\, t_4\right]^{\rm T}, \tag{C.25}$$

where

$$\mathbf{Q}_2 = \begin{pmatrix} 6\lambda_1^4\lambda_{30}^4\chi^2\overline{B}_{20} & 3\lambda_1^2\lambda_{30}\left\{5\left(1-\chi\right) + 7\lambda_1^2\lambda_{30}^2\left[\lambda_1^2\left(\chi-1\right) + \chi^2\overline{B}_{20}^2\right]\right\} \\ 2\lambda_{30}^2\chi\overline{B}_{20} & 2\left(2\lambda_{30}^3 + \lambda_{30}\chi\overline{B}_{20}^2\right) \end{pmatrix},$$

$$\begin{aligned}
t_3 = &\left(1 + 3\lambda_1^4\lambda_{30}^2\right)\left(\chi-1\right) + \lambda_1^2\lambda_{30}^2\chi^2\left(3\lambda_1^2\lambda_{30}^2\gamma_1^2 - \overline{B}_{20}^2\right) + \\
&+ 3\lambda_1^2\gamma_2^2\left\{10\left(1-\chi\right) + 21\lambda_1^2\lambda_{30}^2\left[\lambda_1^2\left(\chi-1\right) + \overline{B}_{20}^2\chi^2\right]\right\}
\end{aligned}$$

$$+ 6\lambda_1\gamma_2\left[2+\lambda_1^3\lambda_{30}^2\left(7\lambda_{30}\chi^2\overline{B}_{20}\gamma_1-3\lambda_1\right)\right],$$

$$t_4 = 4\lambda_{30}\chi\overline{B}_{20}\gamma_1\gamma_2+\lambda_{30}^2\chi\gamma_1^2+\left(6\lambda_{30}^2+\chi\overline{B}_{20}^2\right)\gamma_2^2. \tag{C.26}$$

Again, when there is no pre-stretch ($\lambda_1 = 1$), the zero-order thin-plate equations (C.15) and (C.16) yield one root $\overline{B}_{20} = 0$ and $\lambda_{30} = 1$. Hence, the corrections (C.22) and (C.24) give $\overline{B}_2^{\rm cr} \equiv 0$ independent of kH, are not applicable in this case and we need to re-do the expansion. Specifically, expanding the bifurcation equation (C.14) to the third order in kH, and setting $\lambda_1 = 1$, we obtain

$$-2(1+\lambda_3^2)(kH)^3+\lambda_3\left[(\chi-1)(1+3\lambda_3^2)-\overline{B}_2^2\chi^2\lambda_3^2\right](kH)^2 + 3\lambda_3^2(1-\lambda_3^2)kH+3\lambda_3^3\left[(1-\chi)(1-\lambda_3^2)+\overline{B}_2^2\chi^2\lambda_3^2\right]=0. \tag{C.27}$$

Conducting the same operations of Eqs. (C.15) and (C.27) as those in Appendix C.1.2, we finally get

$$\overline{B}_2^{\rm cr} = \frac{2\sqrt{2\left(1-\chi\right)}}{\sqrt{3\chi\left(1+\chi\right)}}kH, \qquad \lambda_3^{\rm cr} = 1+\frac{2\left(\chi-1\right)}{3\left(1+\chi\right)}(kH)^2 \tag{C.28}$$

for the first-order correction of $\overline{B}_2^{\rm cr}$, and

$$\overline{B}_2^{\rm cr} = \frac{2\sqrt{2\left(1-\chi\right)}}{\sqrt{3\chi\left(1+\chi\right)}}kH+\frac{2\sqrt{2\chi\left(1+\chi\right)}}{\left(1+\chi\right)^2\sqrt{3\left(1-\chi\right)}}(kH)^2,$$
$$\lambda_3^{\rm cr} = 1+\frac{2\left(\chi-1\right)}{3\left(1+\chi\right)}(kH)^2-\frac{4\chi}{3(1+\chi)^2}(kH)^3 \tag{C.29}$$

for the second-order correction of $\overline{B}_2^{\rm cr}$.

References

Beatty, M. F., Pan, F., 1998. Stability of an internally constrained, hyperelastic slab. International Journal of Non-Linear Mechanics 33 (5), 867–906.

Brigadnov, I., Dorfmann, A., 2003. Mathematical modeling of magneto-sensitive elastomers. International Journal of Solids and Structures 40 (18), 4659–4674.

Brown, W. F., 1966. Magnetoelastic Interactions. Springer, New York.

Bustamante, R., 2010. Transversely isotropic nonlinear magneto-active elastomers. Acta Mechanica 210 (3-4), 183–214.

Castañeda, P. P., Galipeau, E., 2011. Homogenization-based constitutive models for magnetorheological elastomers at finite strain. Journal of the Mechanics and Physics of Solids 59 (2), 194–215.

Dalrymple, J. M., Peach, M. O., Viegelahn, G. L., 1974. Magnetoelastic buckling of thin magnetically soft plates in cylindrical mode. Journal of Applied Mechanics 41 (1), 145–150.

Danas, K., Triantafyllidis, N., 2014. Instability of a magnetoelastic layer resting on a non-magnetic substrate. Journal of the Mechanics and Physics of Solids 69, 67–83.

Destrade, M., Ogden, R. W., 2011. On magneto-acoustic waves in finitely deformed elastic solids. Mathematics and Mechanics of Solids 16 (6), 594–604.

Dorfmann, A., Ogden, R., 2004. Nonlinear magnetoelastic deformations. Quarterly Journal of Mechanics and Applied Mathematics 57 (4), 599–622.

Dorfmann, L., Ogden, R. W., 2014. Nonlinear Theory of Electroelastic and Magnetoelastic Interactions. Springer, New York.

Flavin, J., 1963. Surface waves in pre-stressed Mooney material. The Quarterly Journal of Mechanics and Applied Mathematics 16 (4), 441–449.

Galipeau, E., Rudykh, S., deBotton, G., Castañeda, P. P., 2014. Magnetoactive elastomers with periodic and random microstructures. International Journal of Solids and Structures 51 (18), 3012–3024.

Gerbal, F., Wang, Y., Lyonnet, F., Bacri, J.-C., Hocquet, T., Devaud, M., 2015. A refined theory of magnetoelastic buckling matches experiments with ferromagnetic and superparamagnetic rods. Proceedings of the National Academy of Sciences 112 (23), 7135–7140.

Ginder, J., Clark, S., Schlotter, W., Nichols, M., 2002. Magnetostrictive phenomena in magnetorheological elastomers. International Journal of Modern Physics B 16, 2412–2418.

Ginder, J. M., Schlotter, W. F., Nichols, M. E., 2001. Magnetorheological elastomers in tunable vibration absorbers. Proceedings SPIE 4331, 103–110.

Goshkoderia, A., Chen, V., Li, J., Juhl, A., Buskohl, P., Rudykh, S., 2020. Instability-induced pattern formations in soft magnetoactive composites. Physical Review Letters 124 (15), 158002.

Hoang, N., Zhang, N., Du, H., 2010. An adaptive tunable vibration absorber using a new magnetorheological elastomer for vehicular powertrain transient vibration reduction. Smart Materials and Structures 20 (1), 015019.

Kankanala, S., Triantafyllidis, N., 2004. On finitely strained magnetorheological elastomers. Journal of the Mechanics and Physics of Solids 52 (12), 2869–2908.

Kankanala, S., Triantafyllidis, N., 2008. Magnetoelastic buckling of a rectangular block in plane strain. Journal of the Mechanics and Physics of Solids 56 (4), 1147–1169.

Karami Mohammadi, N., Galich, P. I., Krushynska, A. O., Rudykh, S., 2019. Soft magnetoactive laminates: Large deformations, transverse elastic waves and band gaps tunability by a magnetic field. Journal of Applied Mechanics 86 (11).

Kim, Y., Yuk, H., Zhao, R., Chester, S. A., Zhao, X., 2018. Printing ferromagnetic domains for untethered fast-transforming soft materials. Nature 558 (7709), 274–279.

Lanotte, L., Ausanio, G., Hison, C., Iannotti, V., Luponio, C., 2003. The potentiality of composite elastic magnets as novel materials for sensors and actuators. Sensors and Actuators A: Physical 106 (1-3), 56–60.

Lefèvre, V., Danas, K., Lopez-Pamies, O., 2017. A general result for the magnetoelastic response of isotropic suspensions of iron and ferrofluid particles in rubber, with applications to spherical and cylindrical specimens. Journal of the Mechanics and Physics of Solids 107, 343–364.

Lefèvre, V., Danas, K., Lopez-Pamies, O., 2020. Two families of explicit models constructed from a homogenization solution for the magnetoelastic response of MREs containing iron and ferrofluid particles. International Journal of Non-Linear Mechanics 119, 103362.

Luo, Z., Evans, B. A., Chang, C.-H., 2019. Magnetically actuated dynamic iridescence inspired by the neon tetra. ACS Nano 13 (4), 4657–4666.

Makarova, L. A., Alekhina, Y. A., Rusakova, T. S., Perov, N. S., 2016. Tunable properties of magnetoactive elastomers for biomedical applications. Physics Procedia 82, 38–45.

Martin, J. E., Anderson, R. A., Read, D., Gulley, G., 2006. Magnetostriction of field-structured magnetoelastomers. Physical Review E 74 (5), 051507.

Maugin, G. A., 1988. Continuum Mechanics of Electromagnetic Solids. North-Holland, Amsterdam.

Miya, K., Hara, K., Someya, K., 1978. Experimental and theoretical study on magnetoelastic buckling of a ferromagnetic cantilevered beam-plate. Journal of Applied Mechanics 45, 355–360.

Moon, F. C., Pao, Y.-H., 1968. Magnetoelastic buckling of a thin plate. Journal of Applied Mechanics 35, 53–58.

Mukherjee, D., Bodelot, L., Danas, K., 2020. Microstructurally-guided explicit continuum models for isotropic magnetorheological elastomers with iron particles. International Journal of Non-Linear Mechanics 120, 103380.

Otténio, M., Destrade, M., Ogden, R. W., 2008. Incremental magnetoelastic deformations, with application to surface instability. Journal of Elasticity 90 (1), 19–42.

Pao, Y.-H., Yeh, C.-S., 1973. A linear theory for soft ferromagnetic elastic solids. International Journal of Engineering Science 11 (4), 415–436.

Popelar, C. H., 1972. Postbuckling analysis of a magnetoelastic beam. Journal of Applied Mechanics 39, 207–212.

Psarra, E., Bodelot, L., Danas, K., 2017. Two-field surface pattern control via marginally stable magnetorheological elastomers. Soft Matter 13 (37), 6576–6584.

Psarra, E., Bodelot, L., Danas, K., 2019. Wrinkling to crinkling transitions and curvature localization in a magnetoelastic film bonded to a non-magnetic substrate. Journal of the Mechanics and Physics of Solids 133, 103734.

Rambausek, M., Keip, M.-A., 2018. Analytical estimation of non-local deformation-mediated magneto-electric coupling in soft composites. Proceedings of the Royal Society A: Mathematical, Physical and Engineering Sciences 474 (2216), 20170803.

Reddy, N. H., Saxena, P., 2018. Instabilities in the axisymmetric magnetoelastic deformation of a cylindrical membrane. International Journal of Solids and Structures 136, 203–219.

Rigbi, Z., Jilken, L., 1983. The response of an elastomer filled with soft ferrite to mechanical and magnetic influences. Journal of Magnetism and Magnetic Materials 37 (3), 267–276.

Rudykh, S., Bertoldi, K., 2013. Stability of anisotropic magnetorheological elastomers in finite deformations: A micromechanical approach. Journal of the Mechanics and Physics of Solids 61 (4), 949–967.

Saxena, P., Hossain, M., Steinmann, P., 2013. A theory of finite deformation magneto-viscoelasticity. International Journal of Solids and Structures 50 (24), 3886–3897.

Shuvalov, A., Poncelet, O., Deschamps, M., 2004. General formalism for plane guided waves in transversely inhomogeneous anisotropic plates. Wave Motion 40 (4), 413–426.

Singh, R., Onck, P., 2018. Magnetic field induced deformation and buckling of slender bodies. International Journal of Solids and Structures 143, 29–58.

Su, Y., Broderick, H. C., Chen, W., Destrade, M., 2018. Wrinkles in soft dielectric plates. Journal of the Mechanics and Physics of Solids 119, 298–318.

Su, Y., Chen, W., Dorfmann, L., Destrade, M., 2020. The effect of an exterior electric field on the instability of dielectric plates. Proceedings of the Royal Society A 476 (2239), 20200267.

Su, Y., Wu, B., Chen, W., Destrade, M., 2019. Finite bending and pattern evolution of the associated instability for a dielectric elastomer slab. International Journal of Solids and Structures 158, 191–209.

Tang, J., Qiao, Y., Chu, Y., Tong, Z., Zhou, Y., Zhang, W., Xie, S., Hu, J., Wang, T., 2019. Magnetic double-network hydrogels for tissue hyperthermia and drug release. Journal of Materials Chemistry B 7 (8), 1311–1321.

Tian, T., Li, W., Deng, Y., 2011. Sensing capabilities of graphite based MR elastomers. Smart materials and structures 20 (2), 025022.

Tiersten, H., 1964. Coupled magnetomechanical equations for magnetically saturated insulators. Journal of Mathematical Physics 5 (9), 1298–1318.

Wallerstein, D. V., Peach, M. O., 1972. Magnetoelastic buckling of beams and thin plates of magnetically soft material. Journal of Applied Mechanics 39, 451–455.

Yu, K., Fang, N. X., Huang, G., Wang, Q., 2018. Magnetoactive acoustic metamaterials. Advanced Materials 30 (21), 1706348.